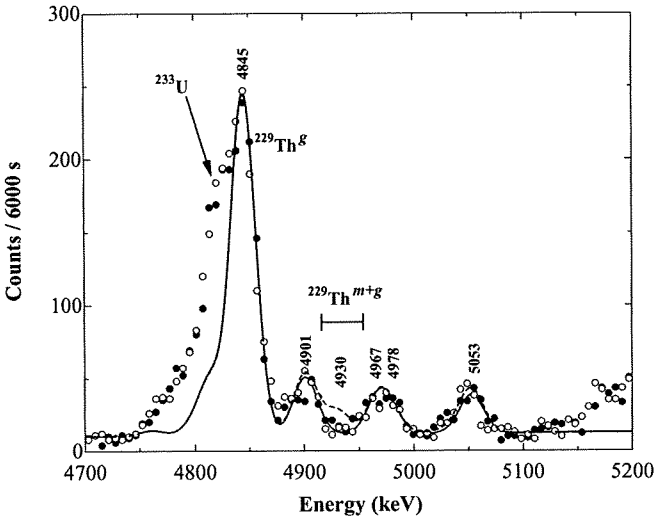

FIG. 3. A magnification of the α-particle spectrum for the region related to ^{229}Th. The solid circles show counts per channel for the initial 6000 s and the open circles show counts per channel for the following 6000 s. The lines drawn in the figures are the same as those in Fig. 1 (see text for detail).

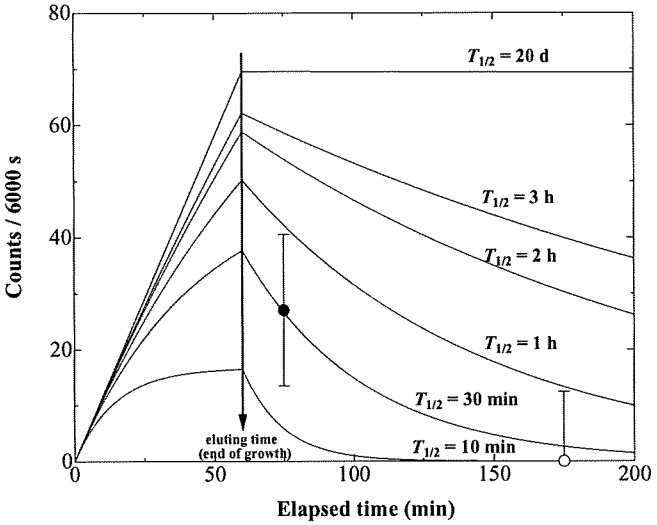

FIG. 4. Estimated growth curves in α counts in the energy region of the ^{229}Th^m α particle. Each of the six solid curves represents the expected counts of ^{229}Th^m with a half-life between 10 min and 20 d. The solid and open circles indicate the ^{229}Th^m α counts of the spectrum measured for the initial 6000 s and those for the following 6000 s, respectively.

By contrast, obtained counts of ^{229}Th^g were 1700 counts per 6000 s. The obtained counts are compatible with the expected counts considering the chemical yield in purification procedures. The ratio of the α counts of ^{229}Th^g/^{228}Th was about 1/30, which is consistent with the ratio of the α counts of ^{229}Th^g ($T_{1/2}$ = 7880 y [13]) and ^{228}Th ($T_{1/2} = 1.9116$ y [10]) estimated from the ^{233}U ($T_{1/2} = 1.592 \times 10^5$ y [10]) atoms containing the ^{232}U ($T_{1/2} = 68.9$ y [10]) atoms at 3.17 ppm. The dashed line shows a spectrum that is the sum of the solid line and 2% of ^{229}Th^m as well as Fig. 1. Assuming that ^{229}Th^m is stable for isomeric transition or that it has a half-life longer than a few days, one expects to obtain a spectrum corresponding with the dashed line. However, the obtained spectrum is close to the solid line, which indicates that ^{229}Th^m scarcely remained at the measurement.

To estimate the half-life of ^{229}Th^m, in Fig. 4 we show the α counts in the region of 4915–4955 keV (hereinafter called the ROI, region of interest), where the main peak of ^{229}Th^m is expected to appear, as a function of elapsed time. As with Fig. 3, the solid and open circles indicate the ROI counts of the spectrum measured for the first 6000 s and for the next 6000 s, respectively. The solid lines show the growth curves of the ROI counts with various half-life values expected as described below. Thorium isotopes were eluted from the anion-exchange column adsorbing ^{233}U at the time when the curves turn off. Until this time, ^{229}Th^{m,g} increase because of the decay of ^{233}U, and the number of atoms is given by the following equations:

$$N_m(t) = \frac{\lambda_{233}}{\lambda_m - \lambda_{233}} N_{233} \mathrm{br}_m (e^{-\lambda_{233} t} - e^{-\lambda_m t}), \quad (1)$$

$$N_g(t) = \frac{\lambda_{233}}{\lambda_g - \lambda_{233}} N_{233}(1 - \mathrm{br}_m)(e^{-\lambda_{233} t} - e^{-\lambda_g t}) + \frac{\lambda_m}{\lambda_g - \lambda_m} N_m (e^{-\lambda_m t} - e^{-\lambda_g t}), \quad (2)$$

where N_m, N_g, and N_{233} are the numbers of ^{229}Th^m, ^{229}Th^g, and ^{233}U atoms, respectively, λ_m, λ_g, and λ_{233} are the decay constants of ^{229}Th^m, ^{229}Th^g, and ^{233}U, respectively, and br$_m$ is the branching ratio of the decay of ^{233}U via ^{229}Th^m. And then the ^{229}Th^m component disintegrates to ^{229}Th^g according to its half-life. Here, the ROI counts are given by

$$\text{ROI counts} = \text{eff}\left\{I_m \lambda_{m\alpha} N_m(t) + I_g \lambda_g N_g(t)\right\} + \text{BKG}, \quad (3)$$

where eff is the total efficiency, which is 3.4% in this case, I_m and I_g are the intensities of ^{229}Th^m and ^{229}Th^g in the ROI region, respectively, $\lambda_{m\alpha}$ is the partial α-decay constant of ^{229}Th^m, and BKG is the constant-background counts in the ROI region. The partial half-life of α decay of ^{229}Th^m is estimated to be 2000 y from Refs. [7,11]. According to Refs. [10,11], the ratio of I_m to I_g is 22.8 : 1. The value of eff$\{\lambda_g N_g(t)\}$ + BKG is fitted to the solid line in Fig. 3. Although the first observed value is reproduced most likely with the curve for a half-life of 30 min, no influence of ^{229}Th^m is observed on the second value. The 3σ confidence level of both values gives an upper limit of 2 h for the half-life of ^{229}Th^m. The result is consistent with the upper limit of the short-lived case in Ref. [6], namely, 6 h.

We note that the half-life of ^{229}Th^m may change depending on its chemical form. In this study, the ^{229}Th atoms formed chloride complexes before the α-source preparation and then hydroxides for α-particle spectrum accumulation. Therefore, the present results show the half-life of ^{229}Th^m is less than 2 h under the chemical condition of at least either chloride or hydroxide.

In the framework of a single-particle transition model, the radioactive transition probability via direct photon emission is

given by the following equation:

$$\lambda = \frac{\ln 2}{T_{1/2}} = \frac{8\pi(L+1)}{L[(2L+1)!!]^2} E_\gamma^{2L+1} B(ML), \quad (4)$$

where $T_{1/2}$ is the half-life of a nuclear transition, L is the multipolarity, E_γ is an excited energy of a level, and $B(ML)$ is the reduced transition probability of the nucleus. The excitation energies of $^{229}Th^m$ were reported to be 3.5 ± 1.0 eV [1], 3.4 ± 1.8 eV [2], 5.5 ± 1.0 eV [3], and 7.6 ± 0.5 eV [4]. However, the reduced transition probability of $^{229}Th^m$ to $^{229}Th^g$, $B(M1; +3/2 \rightarrow +5/2)$, was estimated to be 0.043 μ_N^2 [2]. Hence, the partial half-life of $^{229}Th^m$ for direct photon emission is estimated to be between 29 min and 16 h in the energy range from 2.5 to 8.1 eV in a vacuum in the framework of a single-particle transition model.

The partial half-life of less than 2 h corresponds to the excitation energy of higher than 5 eV. Therefore, if the excitation energy of $^{229}Th^m$ is lower than 5 eV, for example, 3.5 eV as reported in Ref. [1], the present results suggest that $^{229}Th^m$ should decay via not only the direct photon emission but also other decay channels, such as an electron bridge mechanism [14] and a medium effect [5]. In contrast, assuming that the excitation energy of $^{229}Th^m$ is larger than 5 eV, the obtained limit of the half-life of $^{229}Th^m$ can be explained even if the decay occurs only via the direct photon emission. In other words, the half-life of $^{229}Th^m$ should be shorter than 2 h regardless of the chemical forms of Th for this excitation energy. In particular, if the excitation energy is larger than an electron-binding energy of the outer valence molecular orbital of Th and its compounds, the internal conversion process is possible and the half-life is not to be significantly changed by the variation of chemical form; therefore, the half-live of shorter than 6 h [6] gives agreement with the present results whereas those of longer than 20 d [6] and 13.9 ± 3 h [7] fall outside of the limits of the results.

In conclusion, we have searched for the α events from $^{229}Th^m$ produced from 93 mg of ^{233}U by α-particle spectrometry with rapid source preparation. From the upper limit of such events, it was concluded that the half-life of $^{229}Th^m$ may be less than 2 h. The excitation energy is strongly expected to be determined more accurately by direct photon emission. If one attempts to detect the photon of isomeric transition from $^{229}Th^m$ with excitation energy higher than the electron-binding energy of Th compounds, as the most recent value 7.6 ± 0.5 eV [4], the experimental design for it should be based on the assumption that $^{229}Th^m$ has a half-life shorter than a few hours.

ACKNOWLEDGMENTS

This study was carried out under the Cooperative Research Program of the International Research Center for Nuclear Materials Science, Institute for Materials Research (IMR), Tohoku University.

[1] R. G. Helmer and C. W. Reich, Phys. Rev. C **49**, 1845 (1994).
[2] V. Barci, G. Ardisson, G. Barci-Funel, B. Weiss, O. El Samad, and R. K. Sheline, Phys. Rev. C **68**, 034329 (2003).
[3] Z. O. Guimarães-Filho and O. Helene, Phys. Rev. C **71**, 044303 (2005).
[4] B. R. Beck, J. A. Becker, P. Beiersdorfer, G. V. Brown, K. J. Moody, J. B. Wilhelmy, F. S. Porter, C. A. Kilbourne, and R. L. Kelley, Phys. Rev. Lett. **98**, 142501 (2007).
[5] E. V. Tkalya, Phys. Usp. **46**, 315 (2003).
[6] E. Browne, E. B. Norman, R. D. Canaan, D. C. Glasgow, J. M. Keller, and J. P. Young, Phys. Rev. C **64**, 014311 (2001).
[7] T. Mitsugashira, M. Hara, T. Ohtsuki, H. Yuki, K. Takamiya, Y. Kasamatsu, A. Shinohara, H. Kikunaga, and T. Nakanishi, J. Radiol. Nucl. Chem. **255**, 63 (2003).
[8] H. Kikunaga, Y. Kasamatsu, K. Takamiya, T. Mitsugashira, M. Hara, T. Ohtsuki, H. Yuki, A. Shinohara, S. Shibata, N. Kinoshita, A. Yokoyama, and T. Nakanishi, Radiochim. Acta **93**, 507 (2005).
[9] Y. Kasamatsu, H. Kikunaga, K. Takamiya, T. Mitsugashira, T. Nakanishi, Y. Ohkubo, T. Ohtsuki, W. Sato, and A. Shinohara, Radiochim. Acta **93**, 511 (2005).
[10] R. B. Firestone and V. S. Shirley, Eds., *Table of Isotopes*, 8th ed. (Wiley & Sons, New York, 1996).
[11] A. M. Dykhne and E. V. Tkalya, JETP Lett. **67**, 251 (1998).
[12] H. Kikunaga, Y. Kasamatsu, K. Takamiya, T. Ohtsuki, H. Yuki, A. Yokoyama, T. Nakanishi, and T. Mitsugashira, Appl. Radiat. Isot. **67**, 539 (2009).
[13] S. J. Goldstein, M. T. Murrell, and R. W. Williams, Phys. Rev. C **40**, 2793 (1989).
[14] D. Hinneburg, M. Nagel, and G. Brunner, Z. Phys. A **291**, 113 (1979).

Journal of the Physical Society of Japan
Vol. 78, No. 3, March, 2009, 035003

Production and Decay Properties of ^{263}Hs

Daiya KAJI*, Kouji MORIMOTO, Nozomi SATO[1], Takatoshi ICHIKAWA, Eiji IDEGUCHI[2], Kazutaka OZEKI, Hiromitsu HABA, Hiroyuki KOURA[3], Yuki KUDOU, Akira OZAWA[4], Takayuki SUMITA[5], Takayuki YAMAGUCHI[6], Akira YONEDA, Atsushi YOSHIDA, and Kosuke MORITA

RIKEN Nishina Center, RIKEN, 2-1 Hirosawa, Wako, Saitama 351-0198
[1]*Department of Physics, Tohoku University, Sendai 980-8578*
[2]*Center for Nuclear Study, University of Tokyo, Wako, Saitama 351-0198*
[3]*Advanced Science Research Center, Japan Atomic Energy Agency, Tokai, Ibaraki 319-1195*
[4]*University of Tsukuba, Tsukuba, Ibaraki 305-8571*
[5]*Faculty of Science and Technology, Tokyo University of Science, Noda, Chiba 278-8510*
[6]*Department of Physics, Saitama University, Saitama 338-8570*

(Received November 15, 2008; accepted January 22, 2009; published March 10, 2009)

KEYWORDS: ^{263}Hs, gas-filled recoil ion separator, new isotope, hassium

DOI: 10.1143/JPSJ.78.035003

Since the first hassium ($Z = 108$) isotope of ^{265}Hs, which was produced via the cold fusion reaction of ^{208}Pb(^{58}Fe,n)^{265}Hs, was discovered by Münzenberg *et al.*,[1] six hassium isotopes of ^{264,266,267,269,270,271}Hs have been produced and their decay properties have been investigated in detail.[2–7] The α-decay of ^{263}Hs produced in the ^{209}Bi(^{55}Mn,n) reaction was first suggested by Oganessian *et al.*,[8] although no information about the decay property of ^{263}Hs, such as α-decay energy, was reported. Additionally, the possible production of ^{267}Ds ($Z = 110$) by using the ^{209}Bi(^{59}Co,n)^{267}Ds reaction was also reported by Ghiorso *et al.*[9] The discussion was based on the α-decay daughter of ^{263}Hs and the followed decay chains, although no decay of ^{263}Hs was detected in the study. In this work, our aim was to produce ^{263}Hs directly and to determine its decay properties for the first time.

The experiment was performed at the linear accelerator (RILAC) facility in RIKEN (The Institute of Physical and Chemical Research) from June 19 to 25, 2008. The isotope of ^{263}Hs was produced by two different reactions of ^{206}Pb(^{58}Fe,n) and ^{208}Pb(^{56}Fe,n). The projectiles of ^{58}Fe and ^{56}Fe with the charge state 13+ were extracted from the 18-GHz ECR ion source and accelerated by using the RILAC. The beams of ^{58}Fe with 287.7 MeV and ^{56}Fe with 280.4 MeV were extracted from the RILAC. The absolute accuracy of the beam energy measurement was $\pm$0.3 MeV. The typical beam intensities on the target were 4.5×10^{12} s^{-1} (corresponding to 0.75 pμA) for ^{58}Fe and 2.3×10^{12} s^{-1} (corresponding to 0.38 pμA) for ^{56}Fe.

The target was prepared by vacuum evaporation of metallic ^{206}Pb and ^{208}Pb on a 30 μg/cm^2 carbon backing foil. The target thicknesses were 400 μg/cm^2 for ^{206}Pb (Enrichment 99.3%) and 440 μg/cm^2 for ^{208}Pb (Enrichment 98.4%). A thin protection layer of approximately 10 μg/cm^2 of carbon covers the target surface in the downstream direction. The energy losses of the beam in the target were evaluated to be 3.9 MeV for ^{58}Fe in ^{206}Pb and 4.3 MeV for ^{56}Fe in ^{208}Pb using a stopping power table.[10] The beam energy at the middle of the target was estimated to be 285.0 MeV for ^{58}Fe and 277.5 MeV for ^{56}Fe, which correspond to the excitation energies of 16.2 and 16.0 MeV, respectively, when we use the mass table of Audi and Wapstra[11] for the projectile and target masses and that of Myers and Swiatecki[12] for the compound nucleus. Sixteen targets were mounted on a ϕ30 cm wheel, which rotated at 3000 rpm, to withstand the high intensity beam.

Reaction products were separated in flight from the beams by using a gas-filled recoil ion separator, GARIS, and were guided into a detector box installed at a focal plane of the GARIS. The separator was filled with a helium gas at a pressure of 86 Pa. A magnetic rigidity $B\rho$ was set to 2.05 Tm for ^{263}Hs measurement.

An evaporation residue (ER) and its successive radioactive decays were measured by using a system of TOF detectors and an array of a silicon position-sensitive detector (PSD) array installed at the focal plane of the GARIS. An identification of the products was based on genetic correlations of the mother and daughter nuclei. The energy resolution for decay α-particles measured only by the PSD was 45 keV in FWHM. However, when some energy was measured by the PSD and the remaining energy by one of the surrounding silicon detectors (SSDs), the energy resolution was 80 keV in FWHM. The singles counting rate of the PSD at the typical beam intensity was approximately 5 cps. The main components of the signals were due to the target recoils and scattered beam particles. The counting rate of the decay signals (anti-coincidence with timing counters) was approximately 0.3 cps. The detection system was monitored and calibrated by the α source of ^{241}Am and the ERs from the ^{nat}Ce + ^{58}Fe reaction.

During the 25-h irradiation of ^{206}Pb with the ^{58}Fe beam and 46-h irradiation of ^{208}Pb with the ^{56}Fe beam, 8 decay chains and 1 decay chain, respectively, have been observed. No spontaneous fission (SF) was detected in the measurements followed directly after the ER implantation in the PSD. The observed correlated decay chains are summarized in Table I: in this table, the measured decay energies, the time intervals between events, and the positions of decay events as well as that of the implantation events are indicated. The properties of decay events obtained by the irradiation of ^{58}Fe on ^{206}Pb coincide well with those by the irradiation of ^{56}Fe on ^{208}Pb. All decay chains were assigned to subsequent decays from ^{263}Hs. The decay data obtained in this work are summarized in Table II. As shown in the table, the decay properties of α2 or SF, α3 or SF, and α4 are in agreement with those of ^{259}Sg, ^{255}Rf, and ^{251}No.[13–15] The α3-decay energy of 8.44 MeV with the decay time of 6.195 s (chain 9) was observed in the present ^{208}Pb(^{56}Fe,n) reaction as one decay event, although no α-decay energy of 8.44 MeV was observed according to the reference data.[14] The ^{255}Rf has a small probability of EC decay branching according to the reference data.[14] There is a possibility that this α3-decay comes from the EC decay product ^{255}Lr, which has decay energies of 8.41 and 8.36 MeV with the half-life of 22 s.[15] Three groups of α-decay energies for ^{263}Hs are observed. The mean α-decay energies of the three groups are 10.82,

*E-mail: daiya@riken.jp

Table I. Summary of all correlated decay chains detected in this work. No.: Number of the chain. E_{ER}: Kinetic energy of ER. E: Decay energy of individual events. TOF: Time-of-flight in the 0.295-m flight path measured by the timing counters. P: Position measured from the bottom of the detector. τ: Time difference between events. Assignments for each decay event of $\alpha 1$, $\alpha 2$ or SF, $\alpha 3$ or SF, and $\alpha 4$ are given in the table. The energies are given in MeV, and the kinetic energy of ER and energy of fission fragments are not corrected for pulse height defects.

	ER			$\alpha 1$			$\alpha 2$ or SF			$\alpha 3$ or SF			$\alpha 4$		
				^{263}Hs			^{259}Sg			^{255}Rf (or ^{255}Lr)			^{251}No		
No.	E_{ER} (MeV)	TOF (ns)	P (mm)	E (MeV)	τ (ms)	P (mm)	E (MeV)	τ (ms)	P (mm)	E (MeV)	τ (ms)	P (mm)	E (MeV)	τ (ms)	P (mm)
^{206}Pb(^{58}Fe,n)^{263}Hs reaction															
1	21.89	53.6	38.2	10.53	0.16	37.6	9.63	747	37.9	200	2313	38.1			
2	21.09	54.4	36.0	10.53[a]	0.42	35.9	9.58	379	35.8	8.76[a]	1473	35.5	8.59	498	36.3
3	20.60	54.5	53.0	10.80	0.44	53.1	9.40[a]	453	48.5	8.70	208	53.4			
4	18.74	56.9	32.7	3.52[b]	0.24	32.0	9.70[a]	87	35.5	198	758	32.8			
5	20.93	57.3	50.1	10.62[a]	1.99	51.4	9.64[a]	625	49.5	168	1923	49.9			
6	22.42	55.0	17.7	10.43	0.80	17.4	9.59	1097	17.0	220	717	17.7			
7	19.61	44.3	32.3	10.54	0.63	32.3	9.73[a]	325	31.6	162	1109	32.1			
8	22.45	52.4	26.5	10.32[a]	2.79	28.7	194	2805	26.5						
^{208}Pb(^{56}Fe,n)^{263}Hs reaction															
9	19.59	54.2	49.3	10.84	0.24	49.2	9.46	173	48.8	8.44	6195	49.1			

a) Sum of PSD and SSD signals.
b) Partial energy deposition is expected in the case of escape event emitted under shallow angles.

Table II. Summary of the decay data obtained in this work.

	E_α (MeV)	$T_{1/2}$ (ms)	Branching
^{263}Hs	10.82 (25%)	$0.60^{+0.30}_{-0.15}$	$\alpha = 100\%$
	10.55 (50%)		
	10.37 (25%)		
^{259}Sg	9.64 (75%)	520^{+260}_{-130}	$\alpha = 89\%$
	9.40 (25%)		SF = 11%
^{255}Rf	8.73 (100%)	840^{+510}_{-230}	$\alpha = 25\%$
			SF = 63%
			EC = 12%
^{251}No	8.59 (100%)	350^{+1650}_{-160}	$\alpha = 100\%$

10.55, and 10.37 MeV, respectively. The half-life of ^{263}Hs is determined to be $0.60^{+0.30}_{-0.15}$ ms.

In this experiment, the total beam doses of the ^{58}Fe and ^{56}Fe were 4.1×10^{17} and 6.2×10^{17} ions, respectively. The production cross sections corresponding to the 8 decay chains and 1 decay chain were evaluated to be 21^{+10}_{-8} and $1.6^{+3.7}_{-1.3}$ pb by assuming the transmission of the system to be 80%. The large difference in the deduced cross sections for the ^{206}Pb + ^{58}Fe and ^{208}Pb + ^{56}Fe reactions can be qualitatively explained by considering the following. The interaction barriers B_{int} defined by Bass[16] for the ^{206}Pb + ^{58}Fe and ^{208}Pb + ^{56}Fe reactions are calculated to be 226.5 and 227.0 MeV, respectively. On the other hand, the reaction energies in the centre of mass frame (E_{cm}) have been set to 222.1 and 218.4 MeV for the ^{206}Pb + ^{58}Fe and ^{208}Pb + ^{56}Fe reactions, respectively, in order to populate the common compound nucleus, ^{264}Hs, at the same excitation energy of 16 MeV. For the ^{206}Pb + ^{58}Fe reaction, the value of $B_{int} - E_{cm}$ is 4.9 MeV, while that for the ^{208}Pb + ^{56}Fe reaction is 8.6 MeV. In these sub-barrier energy fusion reactions, this energy difference can affect the ER cross section significantly. Consequently, the cross section for the ^{206}Pb + ^{58}Fe reaction is larger than that for the ^{208}Pb + ^{56}Fe reaction. However, it is difficult to discuss this matter quantitatively because the measurements were carried out only at one energy level for both reactions. The measurement of excitation functions is necessary for further discussions.

Acknowledgments

This experiment was carried out at the RI Beam Factory operated by the RIKEN Nishina Center and CNS, University of Tokyo. The authors are extremely grateful to Professors Y. Yano and M. Ishihara for their continuous support, encouragement, and useful suggestions. The authors would like to thank Dr. M. Kase and Dr. T. Suda for their support and arrangement of the beamtime and Professor T. Chihara and Dr. N. Suzuki for synthesizing ferrocene for the ion-source material. The authors are also grateful to all accelerator staff for their excellent assistance during the experiment. This research was partially supported by a Grant-in-Aid for Specially Promoted Research, 19002005, 2007, from the Ministry of Education, Culture, Sports, Science and Technology, Japan.

1) G. Münzenberg *et al.*: Z. Phys. A **317** (1984) 235.
2) G. Münzenberg *et al.*: Z. Phys. A **324** (1986) 489.
3) S. Hofmann *et al.*: Eur. Phys. J. A **10** (2001) 5.
4) Yu. A. Lazarev *et al.*: Phys. Rev. Lett. **75** (1995) 1903.
5) S. Hofmann *et al.*: Z. Phys. A **354** (1996) 229.
6) J. Dvorak *et al.*: Phys. Rev. Lett. **97** (2006) 242501.
7) J. Dvorak *et al.*: Phys. Rev. Lett. **100** (2008) 132503.
8) Yu. Ts. Oganessian *et al.*: Z. Phys. A **319** (1984) 215.
9) A. Ghiorso *et al.*: Phys. Rev. C **51** (1995) R2293.
10) L. C. Northcliffe and R. F. Schilling: Nucl. Data Tables A **7** (1970) 233.
11) G. Audi and A. H. Wapstra: Nucl. Phys. A **565** (1993) 1.
12) W. D. Myers and W. J. Swiatecki: Nucl. Phys. A **601** (1996) 141.
13) G. Münzenberg *et al.*: Z. Phys. A **322** (1985) 227.
14) F. P. Heßberger *et al.*: Eur. Phys. J. A **30** (2006) 561.
15) *Table of Isotopes*, ed. R. B. Firestone and V. S. Shirley (Wiley, New York, 1996) 8th ed.
16) R. Bass: Nucl. Phys. A **231** (1974) 45.

Journal of the Physical Society of Japan
Vol. 78, No. 6, June, 2009, 064201

Decay Properties of ^{266}Bh and ^{262}Db Produced in the ^{248}Cm + ^{23}Na Reaction

Kosuke MORITA[1*], Kouji MORIMOTO[1], Daiya KAJI[1], Hiromitsu HABA[1], Kazutaka OZEKI[1], Yuki KUDOU[1], Nozomi SATO[1,2†], Takayuki SUMITA[1,3], Akira YONEDA[1], Takatoshi ICHIKAWA[1‡], Yasuyuki FUJIMORI[4], Sin-ichi GOTO[5], Eiji IDEGUCHI[6], Yoshitaka KASAMATSU[7§], Kenji KATORI[1], Yukiko KOMORI[8], Hiroyuki KOURA[7], Hisaaki KUDO[9], Kazuhiro OOE[8], Akira OZAWA[10], Fuyuki TOKANAI[4], Kazuaki TSUKADA[7], Takayuki YAMAGUCHI[11], and Atsushi YOSHIDA[1]

[1]*Nishina Center for Accelerator-Based Science, RIKEN, Wako, Saitama 351-0198*
[2]*Department of Physics, Tohoku University, Aoba-ku, Sendai 980-8578*
[3]*Faculty of Science and Technology, Tokyo University of Science, Noda, Chiba 278-8510*
[4]*Department of Physics, Yamagata University, Yamagata 990-8560*
[5]*Center for Instrumental Analysis, Niigata University, Ikarashi, Nishi-ku, Niigata 950-2181*
[6]*Center for Nuclear Study, University of Tokyo, Wako, Saitama 351-0198*
[7]*Japan Atomic Energy Agency, Tokai, Ibaraki 319-1195*
[8]*Department of Chemistry, Osaka University, Toyonaka, Osaka 560-0043*
[9]*Department of Chemistry, Niigata University, Ikarashi, Nishi-ku, Niigata 950-2181*
[10]*University of Tsukuba, Tsukuba, Ibaraki 305-8571*
[11]*Department of Physics, Saitama University, Saitama 338-8570*

(Received March 26, 2009; accepted April 7, 2009; published May 25, 2009)

Decay properties of an isotope ^{266}Bh and its daughter nucleus ^{262}Db produced by the ^{248}Cm(^{23}Na,5n) reaction were studied by using a gas-filled recoil separator coupled with a position-sensitive semiconductor detector. ^{266}Bh was clearly identified from the correlation of the known nuclide, ^{262}Db. The obtained decay properties of ^{266}Bh and ^{262}Db are consistent with those observed in the ^{278}113 chain, which provided further confirmation of the discovery of ^{278}113.

KEYWORDS: ^{266}Bh, ^{262}Db, α-decay, spontaneous fission, gas-filled recoil ion separator, position-sensitive focal plane detector
DOI: 10.1143/JPSJ.78.064201

1. Introduction

The identification of the heaviest nuclides is very difficult because of their extremely small production cross sections. Very heavy nuclides usually form an α-decay chain, and they can be conclusively assigned based on a genetic link to known nuclide(s). A nuclide, ^{266}Bh, is the great-grand-daughter of ^{278}113 that is produced in the ^{209}Bi + ^{70}Zn reaction.[1,2] Thus far, only five atoms have been assigned to ^{266}Bh by direct production.[3,4] Most of the heaviest odd–odd nuclei exhibit rather complicated decay properties. Their main decay modes are α-decay, electron-capture (EC) and spontaneous fission (SF). In many cases, these modes coexist in one nucleus. Furthermore, α-decay energies widely distribute because many low-lying states exist in their daughter nuclei. Therefore, it is difficult to obtain a clear assignment of heavy odd–odd nuclides such as ^{266}Bh. Wilk *et al.*[3] reported the production of ^{266}Bh in the ^{249}Bk + ^{22}Ne reaction by the use of a helium gas-jet technique. They observed one decay chain assigned to one originating from ^{266}Bh (^{266}Bh $\longrightarrow$ ^{262}Db $\longrightarrow$ ^{258}Lr $\longrightarrow$). Qin *et al.*[4] studied the decay properties of ^{266}Bh produced in the ^{243}Am + ^{26}Mg reaction by the use of the gas-jet technique. They observed four α-decay chains originating from ^{266}Bh. In the present work, we performed an experiment with the aim of obtaining an unambiguous assignment of ^{266}Bh by a genetic link. For this purpose, we used a gas-filled recoil ion separator (GARIS) coupled to a position-sensitive focal plane detector (PSD). Using a rotating target of ^{248}Cm, ^{266}Bh was produced for the first time in the ^{248}Cm + ^{23}Na reaction. The main purpose of this work is to provide further confirmation of the production and identification of the isotope ^{278}113.

2. Experimental Procedure

The experiment was performed at the RIKEN Linear Accelerator (RILAC) Facility. A schematic view of the experimental setup is shown in Fig. 1.

A $^{248}Cm_2O_3$ target having a thickness of 350 μg/cm^2 was prepared by electrodeposition onto a titanium backing foil having a thickness of 0.91 mg/cm^2. Six pieces of the target were mounted on a rotating wheel having a diameter of 10 cm. During irradiation, the wheel was rotated at 1000 rpm. Although a maximum of eight pieces of the target could be mounted on the wheel, we used only six pieces because of a lack of the curium material.

A ^{23}Na beam was extracted from RILAC. Beam energies of 126, 130, and 132 MeV were used. The corresponding beam energies at the middle of the target were 121, 124, and 126 MeV, respectively. The ^{23}Na beam was pulsed with micro- and macro-pulse structures. The micro-pulse structure was used to prevent the irradiation of the target frame and the two vacant target positions of the wheel. The micro-pulse structure was synchronized to the rotation of the wheel. In the macro-pulse structure, the beam was ON for 3 s and then OFF for 3 s independently of the micro-pulse

*E-mail: morita@ribf.riken.jp
†Present address: Japan Atomic Energy Agency.
‡Present address: Yukawa Institute for Theoretical Physics, Kyoto University.
§Present address: Nishina Center for Accerelator-Based Science, RIKEN.

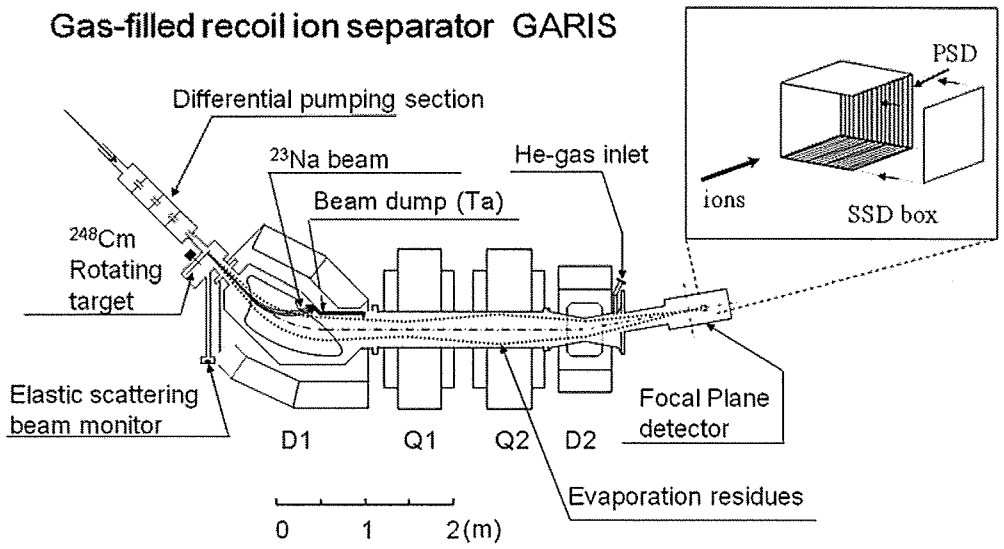

Fig. 1. Schematic view of the experimental setup.

structure. A logical AND signal of the micro- and macro-pulse structures was sent to the beam pulsing system of the accelerator. All the measurements were performed only in the beam OFF period. The counting duty in the macro beam OFF period was 100%, while that in the macro beam ON period was 45%. The beam duty factor was 27.5%. The typical beam intensity was 1 particle-μA on average, and it was 4.4 particle-μA in the micro beam ON period.

GARIS was used to collect evaporation residues (ERs) and separate them from the beam particles and other unwanted charged particles. GARIS was filled with helium gas at a pressure of 33 Pa. Prior to the present experiment, we measured the optimum magnetic rigidity ($B\rho$) for ^{265}Sg produced in the ^{248}Cm(^{22}Ne,5n)^{265}Sg reaction, which differs by only one proton from ^{266}Bh. The highest yield of ^{265}Sg was obtained at 2.07 Tm. Thus, $B\rho$ of GARIS was set at 2.07 Tm for beam energies of 132 and 130 MeV. At beam energies of 126 MeV and a part of 132 MeV, $B\rho$ was set at 2.19 Tm to reduce the counting rate of the focal plane detector to one half.

ERs were transported to the focal plane of GARIS where the PSD was set. The arrangement of the focal plane detector is shown in Fig. 1. The effective area of the PSD is 60 × 60 mm^2. It comprises sixteen strip detectors having a width of 3.75 mm each, and each strip detector has position sensitivity. At a backward of the PSD, semiconductor detectors (SSDs) having the same effective area as the PSD were set in a box shape to detect particles emitted in backward angle from the ERs and their decay daughters.

Because the mass of the projectile is much smaller than that of target for the reaction studied in the present work (asymmetric reaction), the kinetic energy of the ERs is as low as 10 MeV at the focal plane. Consequently, the depth of the implantation into the detector is approximately 1.5 μm. Therefore, if an α-particle is emitted at a backward angle, the energy deposition to the PSD is very small, i.e., a few hundred keV depending on the angle of emission. The position resolving power of the PSD is proportional to the energy deposited in it when the total energy of the α-particle is measured by the sum of PSD and SSD (PSD + SSD event); therefore, in this case, the position resolution becomes poor. A position window should be selected carefully when searching for a correlation event.

The total counting rate of the focal plane detector was approximately 3 × 10^4/s in the beam ON period, while that was 5–10/s in the beam OFF period. Because of the high implantation rate to the PSD in the beam ON period, the PSD was gradually damaged during the measurement. Therefore, the energy resolution of the PSD gradually worsened with time. We replaced the PSD three times during the long experimental period of one and a half months to remove this problem. Energy calibration of the focal plane detectors was performed using long-lived transfer products implanted in the PSD simultaneously with the ERs of interest. The alpha lines used in the calibration were 6.258 MeV (^{248}Cf), 7.039 MeV (^{252}Fm) and 7.192 MeV (^{254}Fm). The energy resolution was measured simultaneously. Occasionally, we also used an ^{241}Am source to check the energy calibration and resolution. An example of a singles spectrum is shown in Fig. 2. The spectrum was obtained from one strip in one run (run161) with a beam dose of 3.1 × 10^{17}. The measurement time was 16.4 h. In the energy region below 8 MeV, α lines from long-lived transfer products are observed, while in the region from 8 to 12 MeV, only one event that was assigned to an α decay of ^{266}Bh was detected.

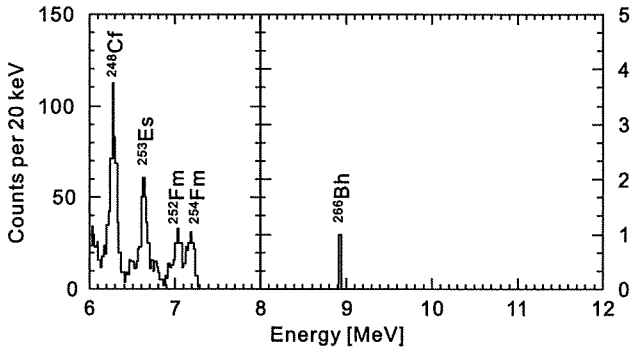

Fig. 2. Example of a singles spectrum for run161. The 7th strip among 16 (0–15) in the PSD was used. The measurement time was 16.4 h for a beam dose of 3.1 × 10^{17}.

Table I. Summary of decay chains observed in the reaction of ^{23}Na on ^{248}Cm.

ID	E_{beam} (MeV)	Strip	E(M) (MeV)	FWHM (MeV)	E(D) (MeV)	FWHM (MeV)	dPos (mm)	τ(D) (s)	E(GD) (MeV)	FWHM (MeV)	dPos (mm)	τ(GD) (s)	Group	Assignment
1	126[a]	2	9.05	0.11	8.71[s]	0.18	−0.45	54.91	8.71	0.11	0.98	9.23	AC	^{266}Bh → ^{262}Db → ^{258}Lr
2	130[b]	11	9.12[s]	0.16	8.74[s]	0.16	3.53	13.76	8.60	0.09	−7.16	9.36	AC	^{266}Bh → ^{262}Db → ^{258}Lr
3	132[a]	7	9.20	0.07	8.67	0.07	0.86	13.71	8.70[s]	0.14	−0.22	4.72	AC	^{266}Bh → ^{262}Db → ^{258}Lr
4	132[a]	7	8.82	0.07	8.54[s]	0.14	1.45	95.45	8.69	0.07	−1.45	3.94	BC	^{266}Bh → ^{262}Db → ^{258}Lr
5	132[b]	13	8.84[s]	0.12	8.42	0.05	−0.12	11.95	169.5[s]		−0.53	27.22	DGI	^{267}Bh → ^{263}Db → ^{259}Lr
6	130[b]	3	9.14	0.12	8.70	0.12	−0.06	66.23					A	^{266}Bh → ^{262}Db or ^{258}Lr
7	132[a]	6	9.23	0.07	8.65	0.07	0.43	22.04					A	^{266}Bh → ^{262}Db or ^{258}Lr
8	132[a]	8	9.14[s]	0.13	8.60	0.06	3.50	7.29					A	^{266}Bh → ^{262}Db or ^{258}Lr
9	132[b]	12	9.22[s]	0.11	8.61	0.04	−0.66	60.40					A	^{266}Bh → ^{262}Db or ^{258}Lr
10	130[b]	10	8.60[s]	0.17	8.70	0.10	−1.72	6.93					C	^{262}Db → ^{258}Lr
11	130[b]	6	8.55	0.09	8.57	0.09	0.12	2.53					C	^{262}Db → ^{258}Lr tentative
12	130[b]	10	8.40	0.11	8.80[s]	0.18	2.99	3.73					C	^{262}Db → ^{258}Lr
13	132[a]	4	8.43	0.10	8.69	0.10	−0.08	5.69					C	^{262}Db → ^{258}Lr
14	132[b]	8	8.84	0.04	8.51	0.04	0.77	82.15					B	^{266}Bh → ^{262}Db tentative
15	126[a]	1	9.07	0.07	154.6[s]		0.52	5.67					E	^{266}Bh → ^{262}Db
16	130[b]	9	9.09[s]	0.15	157.9		−0.56	5.34					E	^{266}Bh → ^{262}Db
17	132[b]	8	9.23	0.06	180.4		1.89	121.53					E	^{266}Bh → ^{262}Db
18	126[a]	7	8.99	0.09	185.8[s]		0.16	8.42					F	^{266}Bh → ^{262}Db tentative
19	126[a]	11	8.97	0.05	157.1		1.53	141.86					F	^{266}Bh → ^{262}Db tentative
20	126[a]	12	8.95[s]	0.13	162.8		−1.56	68.35					F	^{266}Bh → ^{262}Db tentative
21	126[a]	7	8.93	0.08	173.9[s]		0.61	84.30					F	^{266}Bh → ^{262}Db tentative
22	130[b]	7	8.97	0.08	131.1		−1.20	43.99					F	^{266}Bh → ^{262}Db tentative
23	132[a]	1	8.95	0.06	107.5		−0.06	151.36					F	^{266}Bh → ^{262}Db tentative
24	132[b]	13	8.98	0.04	162.8		−0.72	156.99					F	^{266}Bh → ^{262}Db tentative
25	132[b]	10	8.95[s]	0.14	133.8		3.05	26.85					F	^{266}Bh → ^{262}Db tentative
26	126[a]	4	8.76	0.10	124.3[s]		0.14	112.21					H	^{267}Bh → ^{263}Db tentative
27	130[b]	10	8.71	0.08	68.2		0.26	5.38					H	^{267}Bh → ^{263}Db tentative
28	132[b]	11	8.75	0.07	139.9[s]		−0.49	55.57					H	^{267}Bh → ^{263}Db tentative
29	132[b]	10	8.44	0.07	89.4		0.64	35.96					I	^{263}Db or ^{258}Lr
30	130[b]	12	8.84	0.04	173.8[s]		0.76	176.77					G	^{267}Bh → ^{263}Db or ^{259}Lr
31	132[a]	7	8.09	0.07	161.7[s]		−1.52	294.39					J	not assigned
32	132[b]	14	8.09[s]	0.13	164.8[s]		0.28	208.30					J	not assigned

a) Bρ of GARIS was set to 2.19
b) Bρ of GARIS was set to 2.07
s) Sum of PSD and SSD signals

We performed offline analyses to search for mother–daughter correlations, i.e., α-α and α-SF events, based on the position in PSD, energy, and time difference. Because we only considered data from the beam OFF period, a signal indicating the implantation of ER was not recorded. Therefore, the time difference between the ER implantation and its decay event was not obtained.

The average counting rate of particles having energies greater than 50 MeV for each strip of the PSD was 2.7×10^{-4}/s. Considering a positional window of 2 mm, which is a typical position resolution for a true coincidence event for a full energy deposited α-particle and SF, $\pm$1 mm, the counting rate in the positional window is calculated to be 9.3×10^{-6}/s. Considering a time window of 300 s, the probability of an accidental correlation is calculated to be 2.8×10^{-3} per event. This low value of accidental probability was realized by using a combination of GARIS and the PSD. The reduction in the number of transfer products and target recoils at the focal plane that is achieved using the physical pre-separator, GARIS and the high spatial resolving power of the PSD enables a low background α-SF correlation measurements. The α-SF correlation measurement would be difficult to perform using only the gas-jet technique.

3. Results and Discussion

We have assigned total of 32 correlations to true ones. All the correlated events are listed in Table I. The event ID#, beam energies from the accelerator, strip number of the PSD, decay energies and the energy resolutions (in full width at half maximum, FWHM), position difference (in mm), grouping in correlation map mentioned below and assignments for each event are listed. Four of the events are α_1-α_2-α_3 correlations (ID#1–ID#4), one is an α_1-α_2-SF (ID#5), nine are α_1-α_2 (ID#6–ID#14) and eighteen are α_1-SF correlations (ID#15–ID#32). The maximum correlation time was set to 300 s. The position window was set to $\pm$2 mm for the correlation events measured only in the PSD (PSD events). The position window was properly selected for every PSD + SSD event. The superscript "s" in the energy indicated that the event was a PSD + SSD event. A two-dimensional representation of the time- and position-corre-

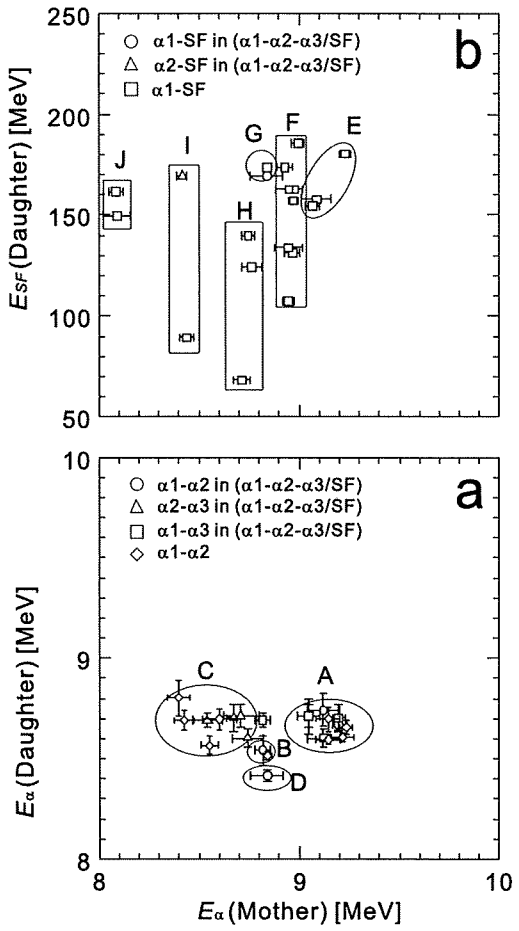

Fig. 3. Two-dimensional representation of time- and position-correlated events. The lower panel (a) shows the α-α correlations. The upper panel (b) shows the α-SF correlations. The time window was set to 300 s.

lated events is shown in Fig. 3. The horizontal and vertical axes represent the mother and daughter energy, respectively. The lower and upper panels [Figs. 3(a) and 3(b)] show the α-α and α-SF correlations, respectively.

The excitation energies of the compound nucleus, ^{271}Bh, at the middle of the target were calculated to be 44.4, 48.1, and 49.9 MeV for beam energies of 126, 130, and 132 MeV, respectively, by using a theoretical mass for ^{271}Bh.[5] The energies were selected to maximize the $5n$ evaporation channel in the ^{248}Cm + ^{23}Na reaction in order to produce the isotope ^{266}Bh. Because the ER cross sections of these asymmetric reactions in the heaviest region exhibit a broad peaks around the optimum energies that produce the maximum yields, the isotope ^{267}Bh, which is a product of the $4n$ evaporation channel of the reaction, could be produced in considerable ammounts, especially at lower excitation energies. We focused on these two isotopes in the analyses. The direct productions of ^{262}Db and ^{263}Db, which are the α-decay daughters of ^{266}Bh and ^{267}Bh by the $\alpha + 5n$ and $\alpha + 4n$ evaporation channels, respectively, were not considered because of the reaction in the sub-barrier energy region.

3.1 α-α correlations

In the correlations shown in Fig. 3(a), eight points are plotted in Group C (ID#1–ID#4, ID#10–ID#13). The mother energies of these events range from 8.40 to 8.74 MeV, and those of the corresponding daughters range from 8.57 to 8.80 MeV. We assigned these events to the ^{262}Db $\longrightarrow$ ^{258}Lr $\longrightarrow$ decay. The average time differences between mother and daughter decays, i.e. the mean life of the daughter nuclide, was calculated to be $5.8^{+3.2}_{-1.5}$ s. The half-life $T_{1/2}$ is deduced to be $4.0^{+2.2}_{-1.0}$ s. The obtained $T_{1/2}$ in this work agrees very well with the adopted value of ^{258}Lr, $3.92^{+0.35}_{-0.42}$ s.[6] The adopted α-decay energies of ^{262}Db are 8.45 ± 0.02, 8.53 ± 0.02, and 8.67 ± 0.02 MeV, and those of ^{258}Lr are 8.565 ± 0.025, 8.595 ± 0.010, 8.621 ± 0.010, and 8.654 ± 0.010 MeV.[6] It should be noted that the α energies obtained in this work are approximately 40–60 keV higher than the adopted energies. This is most probably attributable to the summing of α-energy and a conversion electron or γ-ray energy, which is emitted simultaneously with the α-decay in the cases of odd and odd–odd nuclei.[7] In all previous studies to determine the α-decay energies of ^{262}Db and ^{258}Lr, atoms of these isotopes were collected on a plate or a film by using, for example, the gas-jet technique, and they were not implanted in the detector used. The sources of α-decay were thus outside the detectors. Therefore, this summing effect was not very serious in the previous studies. Because of a shift in energy and the limited energy resolution caused by the summing effect, event ID#11 in Group C could be assigned to the decay of ^{263}Db $\longrightarrow$ ^{259}Lr $\longrightarrow$ as well as that of ^{262}Db $\longrightarrow$ ^{258}Lr $\longrightarrow$. The energies of α_1 and α_2 were measured to be 8.55 (0.09) and 8.57 (0.10) MeV, respectively. The numbers in parentheses indicate the energy resolutions in FWHM. The time difference between the two was 2.5 s. The reported half-life and α-decay energy of ^{263}Db are 27^{+10}_{-7} s and 8.36 MeV[8] and those of ^{259}Lr are $6.34^{+0.46}_{-0.42}$ s and 8.45 MeV,[9] respectively.

Three of the eight correlations in Group C (ID#1, ID#2, and ID#3) are the second part (α_2-α_3) of the triple correlations (α_1-α_2-α_3). All the preceding correlations (α_1-α_2) are in Group A, as shown in Fig. 3(a), along with four additional α_1-α_2 correlations (ID#6–ID#9). Because of the genetic correlation to the ^{262}Db $\longrightarrow$ ^{258}Lr $\longrightarrow$ decay, these three triple correlation events in Group A are conclusively identified as the correlations of ^{266}Bh $\longrightarrow$ ^{262}Db $\longrightarrow$ ^{258}Lr $\longrightarrow$ decays. The other four correlations are identified as those of the ^{266}Bh $\longrightarrow$ ^{262}Db $\longrightarrow$ decay or the ^{266}Bh $\longrightarrow$ (^{262}Db $\longrightarrow$ missing) ^{258}Lr $\longrightarrow$ decay partly because the daughter energies, which range from 8.60 to 8.66 MeV, agree well with the adopted decay energies of ^{262}Db and ^{258}Lr considering the above mentioned summing effect. The mean time differences between the α_1 and α_2 decays of the seven correlations in this group are calculated to be 34^{+20}_{-10} s. The corresponding $T_{1/2}$ is 24^{+14}_{-7} s. This value is attributable to a mixture of the ^{266}Bh $\longrightarrow$ ^{262}Db $\longrightarrow$ and ^{266}Bh $\longrightarrow$ (^{262}Db $\longrightarrow$) ^{258}Lr $\longrightarrow$ decays. Including this mixture effect, the value agrees well with the adopted half-lives of ^{262}Db (34 ± 4 s) and ^{258}Lr ($3.92^{+0.35}_{-0.42}$ s). The observed α-decay energies of ^{266}Bh range from 9.05 to 9.23 MeV. The correlations observed and assigned here agree well with those reported by Wilk *et al.*[3] and Qin *et al.*[4]

One α_1-α_2 correlation of the triple α correlation (ID#4) exists in Group B, as shown in Fig. 3(a). The corresponding α_2-α_3 correlation (ID#4) exists in Group C, suggesting that

the correlations in Group B also correspond to the decay ^{266}Bh $\longrightarrow$ ^{262}Db $\longrightarrow$ ^{258}Lr $\longrightarrow$. The energies of α_2 and α_3 were 8.54 (0.14) and 8.69 (0.07) MeV, respectively. These energies agree well with the reported values for ^{262}Db and ^{258}Lr mentioned above. The observed α energy of ^{266}Bh assigned here is 8.83 MeV. Although the value just coincides with the decay energy of ^{267}Bh reported by Wilk *et al.*,[3] because of the observed decay characteristics, we assigned the correlated event to the decay of ^{266}Bh $\longrightarrow$ ^{262}Db $\longrightarrow$ ^{258}Lr $\longrightarrow$.

One additional correlation (ID#14) exists in Group B, as shown in Fig. 3(a). This could be also assigned to the decay of ^{266}Bh $\longrightarrow$ ^{262}Db $\longrightarrow$ ^{258}Lr $\longrightarrow$ because of the similarity with the energies and decay times of the correlation assigned above. However, based on the α_1-α_2 correlation analysis, assignment to the decay of ^{267}Bh $\longrightarrow$ (^{263}Db $\longrightarrow$) ^{259}Lr $\longrightarrow$ is also possible if the summing effect is considered. Therefore, this correlation could not be assigned conclusively.

α_1-α_2 of one α_1-α_2-SF triple correlation (ID#5) is classified in a circle marked by D in Fig. 3(a). Here, the mother and daughter energies are 8.84 and 8.42 MeV, respectively. The time difference between these decays was 12.0 s. These values, along with the followed SF decay with a decay time of 27.2 s, are fully consistent with the decay of ^{267}Bh $\longrightarrow$ ^{263}Db $\longrightarrow$ ^{259}Lr (SF).[3,9] The reported $T_{1/2}$ values of ^{263}Db and ^{259}Lr are 27^{+10}_{-7} s and 6.2 ± 0.3 s, respectively. We then assign this correlation to the decay originating from ^{267}Bh.

3.2 α-SF correlations

The three correlated events (ID#15, ID#16, and ID#17) in Group E in Fig. 3(b) correspond to the α_1 energies of Group A (9.05–9.23 MeV). The corresponding half-life $T_{1/2}$ deduced from the three events is 31^{+41}_{-11} s, which agrees well with that of ^{262}Db, i.e., 34 ± 4 s. Therefore, we assign these correlated events to SF decays of ^{262}Db fed by 9.05–9.23 MeV α-decays of ^{266}Bh.

Eight correlations (ID#18–ID#25) are observed in Group F in Fig. 3(b). The α-decay energies of the mother range from 8.93 to 8.99 MeV. $T_{1/2}$ of the SF decay is 59^{+32}_{-15} s. No α-decays are observed in the α_1-α_2 correlations in this energy range, as shown in Fig. 3(a). The observed $T_{1/2}$ is slightly longer than the reported $T_{1/2}$ values of both ^{262}Db, 34 ± 4 s, and ^{263}Db, 27^{+10}_{-7} s. Two α-decay events having an energy of around 8.96 MeV were reported by Qin *et al.*,[4] and these are assigned to the decay of ^{266}Bh $\longrightarrow$ ^{262}Db $\longrightarrow$. However, their experimental setup was not sensitive to the α-SF correlations. The α-decays having an energy of around 8.96 MeV observed in the present work fed a state in the daughter that decays mainly by SF with $T_{1/2}$ of 59^{+32}_{-15} s. This α-decay could be tentatively assigned to the ^{266}Bh $\longrightarrow$ ^{262}Db (SF) decay. However, the possibility of assignment to the ^{267}Bh $\longrightarrow$ ^{263}Db (SF) decay could not be excluded. It should be noted that half the correlations were observed at the lowest incident energy.

One correlation (ID#30) exists in Group G, as shown in Fig. 3(b), along with the $\alpha_1(\text{-}\alpha_2)$-SF correlation (ID#5) that was assigned to the decay of ^{267}Bh $\longrightarrow$ ^{263}Db $\longrightarrow$ ^{259}Lr $\longrightarrow$ in the present study. The α_1 energy was 8.84 MeV, and the SF decay time was measured to be 176.8 s, which agree well with those of the correlation ID#5. Then, it is natural to assign this correlation to the decay of ^{267}Bh $\longrightarrow$ ^{263}Db (SF) or ^{267}Bh $\longrightarrow$ ^{263}Db $\longrightarrow$ ^{259}Lr (SF). However, we have assigned one correlation having almost the same α_1 energy to the decay of ^{266}Bh [Group B in Fig. 3(a) (ID#8)], suggesting that the correlation might still be assigned to the decay of ^{266}Bh.

Three correlations (ID#26, ID#27, and ID#28) exist in Group H in Fig. 3(b). The α-decay energy of the mother ranges from 8.71 to 8.76 MeV. The deduced $T_{1/2}$ of the SF decay is 44^{+55}_{-15} s. One decay chain having a decay energy of 8.73 MeV was assigned to the decay of ^{267}Bh by Wilk *et al.*[3] These correlations can possibly be assigned to the decay of ^{267}Bh $\longrightarrow$ ^{263}Db (SF) or ^{267}Bh $\longrightarrow$ (^{263}Db $\longrightarrow$) ^{259}Lr (SF).

Two correlations exist in Group I in Fig. 3(b). The α-decay energy of the mother is approximately 8.43 MeV. One of these correlations is the α_2-SF part of the triple α_1-α_2-SF correlation (ID#5). We have assigned this correlation to the decay of ^{267}Bh $\longrightarrow$ ^{263}Db $\longrightarrow$ ^{259}Lr (SF). The other correlation (ID#30) could also be the decay of ^{263}Db $\longrightarrow$ ^{259}Lr (SF). The mean decay time of the two event is 31.6 s. The corresponding half-life is 22^{+53}_{-9} s. We could tentatively assign these correlations to the decay mentioned above although the deduced SF half-life of ^{259}Lr is slightly longer than the adopted value, 6.2 ± 0.3 s.

Two correlations (ID#31 and ID#32) exist in Group J in Fig. 3(b). The α-decay energy of the mother is approximately 8.09 MeV. The mean value of the decay times is 251 s. Because the maximum correlation time of this analysis is 300 s, we could not determine the decay time of these correlations, and therefore, we could not assign these correlations.

3.3 9.05–9.23 MeV α decay of ^{266}Bh

An isotope of the 107th element, ^{266}Bh, which decays by α-emission with an energy ranging from 9.05 to 9.23 MeV, was conclusively identified by the present study. A state in the daughter nuclei ^{262}Db, fed by the α-decay, decays by α-emission and SF. In the observed decay chains of the isotope of the 113th element, ^{278}113, studied by the RIKEN group,[1,2] one of the great-granddaughters decayed by α-emission with a decay energy of 9.08 MeV and decay time of 2.47 s, followed by SF. The assignment was based on an experimental result of the work done by Wilk *et al.*[3] that reported one atom of ^{266}Bh assigned by the sequential α-decays ^{262}Db $\longrightarrow$ ^{258}Lr $\longrightarrow$. The present work provided further confirmation of the assignment of ^{266}Bh observed in a decay chain originating from ^{278}113 by demonstrating the observation of the same decay energy, as well as the observation of SF decays following the relevant α-decay of ^{266}Bh.

Although a decay time analysis was performed in the macro beam OFF period, because of the small counting statistics, we could only state that the half-life is longer than 1 s.

3.4 Cross section

We calculated an energy-averaged, inclusive cross section for the 30 correlated events assigned to the decays of ^{266}Bh and ^{267}Bh. The counting efficiencies for different correlation types differed from each other. The efficiency is unity for the

α-SF (4 events) correlations, 0.7 for the α-α (12 events) and α-α-SF (one event) correlations, and 0.5 for the α-α-α (16 events) correlations. The counting duty was 0.725. The total beam dose was 1.9×10^{19}, and the target thickness was $7.7 \times 10^{17}/\mathrm{cm}^2$. Assuming the transmission efficiency of GARIS to 0.08, we calculated the cross section to be 50 pb.

4. Conclusion

An isotope of the 107th element, ^{266}Bh, that is produced by the ^{248}Cm(^{23}Na,5n) reaction was clearly identified. The identification was based on a genetic link to the known daughter nucleus ^{262}Db by α-decays. The isotope ^{267}Bh, which is a reaction product of the 4n evaporation channel, was also produced and identified. A state in ^{266}Bh, which decays by an α-emission with the energies ranging from 9.05 to 9.23 MeV, feeds a state in ^{262}Db, which decays by α-emission and by SF with a previously known half-life. The result provided a further confirmation of the production and identification of the isotope of the 113th element, ^{278}113, studied by a research group at RIKEN, Japan.

Acknowledgements

We are grateful to Dr. Y. Yano and Dr. M. Kase for their continuous support, encouragement and useful suggestions. We also thank Dr. O. Kamigaito and all accelerator staff members for their excellent operation for a long period of time. Many thanks are also due to all members of RIKEN Nishina Center for Accelerator-Based Science, for their encouragement and support. We thank all members of RIKEN Headquarter headed by Dr. R. Noyori for their warm support. One of the authors (K. M.) thanks his late wife. This research was partly supported by a Grant-in-Aid for Specially Promoted Research, 10992005, from the Ministry of Education, Culture, Sports, Science and Technology, Japan.

1) K. Morita, K. Morimoto, D. Kaji, T. Akiyama, S. Goto, H. Haba, E. Ideguchi, R. Kanungo, K. Katori, H. Koura, H. Kudo, T. Ohnishi, A. Ozawa, T. Suda, K. Sueki, H. S. Xu, T. Yamaguchi, A. Yoneda, A. Yoshida, and Y. L. Zhao: J. Phys. Soc. Jpn. **73** (2004) 2593.
2) K. Morita, K. Morimoto, D. Kaji, T. Akiyama, S. Goto, H. Haba, E. Ideguchi, K. Katori, H. Koura, H. Kikunaga, H. Kudo, T. Ohnishi, A. Ozawa, N. Sato, T. Suda, K. Sueki, F. Tokanai, T. Yamaguchi, A. Yoneda, and A. Yoshida: J. Phys. Soc. Jpn. **76** (2007) 045001.
3) P. A. Wilk, K. E. Gregorich, A. Türler, C. A. Laue, R. Eichler, V. Ninov, J. L. Adams, U. W. Kirbach, M. R. Lane, D. M. Lee, J. B. Patin, D. A. Shaughnessy, D. A. Strellis, H. Nitsche, and D. C. Hoffman: Phys. Rev. Lett. **85** (2000) 2697.
4) Z. Qin, X.-L. Wu, H.-J. Ding, W.-S. Wu, W.-X. Huang, X.-G. Lei, Y.-B. Xu, X.-H. Yuan, B. Guo, W.-F. Yang, Z.-G. Gan, H.-M. Fan, J.-S. Guo, H.-S. Xu, and G.-Q. Xiao: Nucl. Phys. Rev. **23** (2006) 400 (Chinese journal in English).
5) P. Möller, J. R. Nix, W. D. Myers, and W. J. Swiatecki: At. Data Nucl. Data Tables **59** (1995) 185.
6) R. Dressler, B. Eichler, D. T. Jost, D. Piguet, A. Türler, Ch. Düllmann, R. Eichler, H. W. Gäggeler, M. Gärtner, M. Schädel, S. Taut, and A. B. Yakushev: Phys. Rev. C **59** (1999) 3433.
7) M. Asai, K. Tsukada, M. Sakama, S. Ichikawa, T. Ishii, Y. Nagame, I. Nishinaka, K. Akiyama, A. Osa, Y. Oura, K. Sueki, and M. Shibata: Phys. Rev. Lett. **95** (2005) 102502.
8) J. V. Kratz, M. K. Gober, H. P. Zimmermann, M. Schädel, W. Brüchle, E. Schimpf, K. E. Gregorich, A. Türler, N. J. Hannink, K. R. Czerwinski, B. Kadkhodayan, D. M. Lee, M. J. Nurmia, D. C. Hoffman, H. Gäggeler, D. Jost, J. Kovacs, U. W. Scherer, and A. Weber: Phys. Rev. C **45** (1992) 1064.
9) K. E. Gregorich, H. L. Hall, R. A. Henderson, J. D. Leyba, K. R. Czerwinski, S. A. Kreek, B. A. Kadkhaodayan, M. J. Nurmia, D. M. Lee, and D. C. Haffman: Phys. Rev. C **45** (1992) 1058.

分析測定法

微量元素の分析技術
—臨床検査の実際と今後の展開

五十嵐香織[1)]/榎本秀一[2)]

〔SUMMARY〕 臨床検査における体液中の無機質(金属元素，ミネラル)の分析に関しては，通常，血清中や尿中の分析が日常であろう．体液中の無機質は，遊離型イオンとして存在する Na^+，K^+，Cl^-，HPO_4^{2-}，HCO_3^-，SO_4^{2-} などがあり，これらを電解質と呼んでいる．一方，蛋白質や低分子化合物との結合型や遊離型で存在する Ca^{2+}，Mg^{2+}，蛋白質と結合している場合の多い Fe，Cu，Zn，Mn などが存在するが，これらを微量元素と呼んでいる．本稿では，これら無機質成分のうち特に微量元素の臨床検査に着目し，汎用される分析機器や今後，利用が増していくことが予測される先端分析機器を紹介し，併せて通常汎用される臨床検査法を紹介したい．〔臨床検査　53：185-189，2009〕

〔KEYWORDS〕 原子吸光法，ICP 質量分析法，ICP 発光分析法，スペシエーション，イメージング技術

汎用されている機器分析法

基本的に無機質はナトリウム，カリウム，リンなどのマクロ量存在する元素と生体内に極微量に存在する微量元素とは分析手法が異なる．マクロ量に存在する元素の分析法は，簡便な炎光光度法やイオン電極法のほか，キレート試薬による呈色反応，酵素反応を利用する系などが開発されており，本稿では詳細な解説は割愛した．これらに関しては，臨床検査の成書をご参照いただきたい[1)]．一方，生体内に存在する微量元素の簡便な機器分析法としては，原子吸光法，ICP 発光分析法および ICP 質量分析法が一般的であり，かつ感度も高く汎用されている．以下に，現在臨床検査で使われている機器分析法について概説する．ここに紹介する機器も本稿では要点のみ触れることとしたので，詳しくは優れた成書を参考にされたい[2)]．

1. 原子吸光法，ICP 発光分析法および ICP 質量分析法への試料の前処理

臨床検査における試料は血漿，血清，尿などの体液試料であり，試料前処理は，蛋白質，脂質などの有機物を分解によって取り除き，無機物として元素を分析するために重要な操作となる．

前処理の仕方は，生体試料の場合，湿式灰化法やマイクロウェーブ灰化法が一般的である．これは測定対象元素や使用する分析機器によって最適化した量の試料を精密に計量し，有害金属測定用あるいは精密分析用などの硝酸，硫酸，過塩素酸，過酸化水素などを単独あるいは混合して加え，加熱分解する．この後，定容化して測定試料とする．この方法で用いる酸の種類や組合せは非常に重要であり，そのテクニックは専門書に譲る[2)]．処理に際しては，揮散しやすい元素の損失や使用する試薬に由来する汚染(コンタミネーション)を最小限に抑える必要もあり，操作過程における汚染の問題が常に付きまとい，熟練したオペレーションが重要である．一方，マイクロウェ

1）IGARASHI Kaori　独立行政法人理化学研究所神戸研究所分子イメージング科学研究センターメタロミクスイメージング研究ユニット・研究員
2）ENOMOTO Shuichi　同研究ユニット・ユニットリーダー/岡山大学大学院医歯薬学総合研究科医薬品機能分析学・教授

ーブ灰化法は，試料および酸を入れて密閉したテフロン容器に入れ，マイクロウェーブを照射することにより加熱し，試料を分解する方法である．湿式灰化法に比べ，高温，高圧下で分解するので短時間で分解が完了し，容器が密閉系であるため試料の揮散やコンタミネーションが防止できるなどの利点がある．

2. 原子吸光法(atomic absorption spectrophotometry；AAS)

原子吸光法の原理は，試料溶液中の金属元素を原子化することにより，生じた基底状態の原子が特定の波長の光を吸収する現象を利用する．すなわち，光源から発せられた光量と，試料中の金属濃度に応じて吸収され，検出器に到達した光量との差から求められる吸光度と試料濃度との関係は，Lambert-Beerの法則に従うので，標準液を用いて作成した検量線から未知試料中の金属元素濃度を算出することができる．

原子吸光法は，測定対象とする元素ごとに中空陰極ランプ(測定対象の原子吸光線の波長と一致した波長の光を高輝度で発するランプ)を用いて，原子化させた試料溶液中の元素イオンを定量する方法である．したがって本法は，試料中に含まれる未知元素の同定には適さない．また，後述する多元素同時分析が可能なICP発光分析法やICP質量分析法に対して，原子吸光法は多元素を同時に測定することも理論上不可能である(複数本の中空陰極ランプに複数の検出器を対応させ，数元素の同時分析を可能にした機器も開発されている)．

原子吸光法における原子化の方法にはフレーム法，フレームレス法，還元気化法，水素化物発生法などがある．また，定量法としては，絶対検量線法や標準添加法が利用されている．標準液の作製には既成の原子吸光用標準溶液を利用する．

3. ICP発光分析(inductively coupled plasma-atomic emission spectroscopy)

ICP-AESでは，試料を酸で分解した後，その溶液を6,000℃以上の高温Arプラズマ中に噴霧する．このことで，ほとんどの元素は励起され，原子やイオンに解離され，イオン化発光した光を波長ごとに分光して，その強度を測定する．各元素固有の波長で発光するため，発光波長を掃引するか複数検出器を利用することで，試料中に存在する多数の元素の同時検出，定量が可能である．原子吸光法に比較して，検量線のダイナミックレンジが広く，真空紫外部を測定可能な検出器を備えた機器であれば，硫黄やリンなどの軽元素も検出可能である．定量法としては絶対検量線法や標準添加法が利用できる．標準液の作製には，市販のICP発光分析法用の標準溶液を用い，混合標準液を作製する．ただ，混合による化学反応あるいは測定対象元素やマトリックスの発光線の波長の重なり(スペクトル干渉)に注意を要する．

4. ICP質量分析(inductively coupled plasma-mass spectroscopy)

ICP質量分析法は，1980年ころから初期の装置の報告がなされ，今日では，前述のAASやICP発光分析法などの光学的手法に代わる微量元素分析法として汎用されている．その応用分野は，医学，薬学領域のみならず，半導体研究から，環境科学研究分野にも及んでいる．

測定原理は，ICP発光分析法と同じように，試料を酸で分解した後，その溶液に含まれる元素をArプラズマ中で元素をイオン化し，質量電荷比(m/z)によって分離して，シグナルを増幅後，電気的に計測する．ICP発光分析法と比較すると，多くの元素について2～3桁程度高感度であり，スペクトル干渉がなく，同位体分析も可能である．m/zを掃引し元素固有のm/z値から試料中の元素種を多元素同時に検出でき，そのシグナル強度から定量分析できる．定量法は，絶対検量線法や標準添加法の他，同位体希釈法も利用できる．標準液の作製は，市販のICP質量分析法用標準溶液を利用し，混合による化学反応や測定対象元素どうしの同重体干渉，マトリックスに由来する分子イオン干渉の発生に留意して混合標準溶液を作製する．

生体微量元素は質量数(m/z)が100以下の元素が多いため，ICP質量分析法で測定する場合，プラズマ源(Ar)や分解に使用した後に残存する酸あるいはマトリックスによって生成する分子イオン干渉を回避することが重要である．

5. 今後の利用が期待される最新分析法

1) 化学形態分析(スペシエーション)[3]

化学形態分析(スペシエーション)は，試料中で

様々な化学形態をとっている目的の元素を，様々な原理に基づく分離手法で分離し，元素に特異的に検出するという分析である．元素を特異的に検出するため，生体内で金属の貯蔵や輸送体などのような適切な酸素活性がない金属との結合蛋白質や核酸との複合体あるいは低分子量の金属含有代謝物などを検出する非常に有用な手段となる．

スペシエーションを行うには，化学形，荷電状態，機能ごとに分離し，含まれる金属に特異的な検出方法で検出することが必要である．このように分離の後，特異的な検出を行うため，それぞれ単一機器としても機能分離できる測定機器(高性能液体クロマトグラフィ；HPLC など)と検出のための測定機器(ICP 質量分析法など)をオンラインで組み合わせて用いる．

生体微量元素のスペシエーション分析の分離手法は，多くの生体成分の分離に応用が可能で，様々な分離原理(イオン交換，分子ふるい，吸着，分配など)による分離ができ，分離，検出とも溶液系で行えることなどの制限から，HPLC が最も一般的である．一般に生体内に存在する種々の微量元素は，単独のイオンとして存在するよりもむしろ様々な蛋白質などの生体分子と結合しているような状態で体内を動くことが多く，この際の化学状態の把握や代謝物の追跡の重要性がますます高まっている．このような意味から，今後このスペシエーション分析の一層の研究開発が進むと考えられる．

2）イメージング技術と微量元素の挙動

基礎科学研究者の間で長らく用いられてきたイメージング技術であるが，昨今，この分野の進歩が著しい．今後，新たな疾病診断のパワフルツールとなっていくことが予測され，また，日常の診断や検査の中での重要性が高まっていくであろう．イメージング技術には，蛍光，MRI や核医学のイメージングがあるが，これらの技術は，生体や個体の病態のリアルタイム画像をダイナミックに捉えることができるので，極めて有益な情報をもたらす．

蛍光イメージングは，蛍光を有する化合物と標的分子の相互作用を利用するものであるが，昨今，蛍光分光分析法のうち共焦点レーザー顕微鏡，蛍光相関分光などの機器の研究や開発が進んでおり，新たな蛍光試薬(プローブ)の創薬も進行している．生体元素のうち，Ca，Zn，Mg の蛍光イメージングは，優れた蛍光イメージングプローブの開発がなされ，今日多くの生命現象と微量元素のかかわりあいの解明に用いられている[4]．また，核磁気共鳴によるイメージング MRI は，強力磁石を用いて生体中の水素原子核に強い高周波を照射して，放出される高周波を受信することによるイメージングであるが，生体微量元素の関与する生体反応によって起こされる水分子のダイナミクス変化を評価する以外に，MRI 用造影剤の利用や緩和時間の測定による金属元素の集積性を見ることも可能である[4]．

さらに，核医学における PET(positron emmission tomography)や SPECT(single photon emission computed tomography)などのイメージング法[4]や新規の核医学イメージング法である複数分子同時イメージング法[4]が開発されているが，これらの手法も種々の元素の放射性同位元素を用いることで微量元素の動的挙動をリアルタイムでイメージングできる．今後，これらの分析手法が，臨床医学や日常検査の場で使用されることも多くなっていくであろう．

実際の臨床検査と微量元素測定

1．カルシウム

1）カルシウム値の変動と疾病[5]

体内のカルシウムの 99% が骨に含有されているが，カルシウムイオンは，酵素の活性化，筋収縮，神経興奮伝達など様々な生理機能発現に重要な元素であることは，ご承知の通りである．血中におけるカルシウムは，ほとんどすべてが血漿中に存在し，その 40～50% がアルブミンなどの蛋白質に結合しており，蛋白質濃度や血液 pH の動態と関連があることから，判定にはアルブミン濃度と pH を考慮しなければならない．カルシウムの尿中への排泄量は血中カルシウム濃度の影響を受ける．また，カルシウムは，骨代謝の観点からリンとも関係があり，血清カルシウム濃度の増加に伴いリン濃度は減少するが，有機リン酸エステルからリン酸イオンが遊離し，カルシウムイオン

と結合して骨に沈着することにより，血中カルシウムイオンとリン酸イオンとの溶解積は一定に保たれている．この代謝にはアルカリフォスファターゼが関与する．

これらのように，血中および尿中カルシウム濃度の測定は，内分泌代謝異常，骨代謝異常やカルシウムの吸収障害等の診断においても意義があり，臨床においては通常，カルシウム，リン，アルカリフォスファターゼの動態から総合的に判断することが重要である．

2）カルシウムの測定法[5]

血清カルシウムの日常検査法は*o*-クレゾールフタレインコンプレクソン法(OCPC法)，MXB法，酵素法，アルセナゾⅢ法など多くの方法がある．この中でもOCPC法は，広く利用されている．この手法は，試料中のカルシウムがアルカリ溶液中で*o*-クレゾールフタレインと結合して赤紫色の錯体を形成することを利用し，この赤紫色の吸光度を測定することによりカルシウム量を求める．一方，原子吸光法はアメリカ標準技術局(National Institute of Standards and Technology；NIST)の標準測定法に指定されている方法で，比色法より正確である．また，電極法は，カルシウムイオンの直接測定法として用いられている．

2. 鉄

1）鉄値の変動と疾病[5~7]

体内の鉄は，ヘモグロビンに約60%，フェリチン・ヘモシデリンに約30%，ミオグロビンに約10%存在するが，欠乏，過剰を起こしやすく，性差や個体差が大きいことから，その値には変動が認められる．鉄は，酸素運搬や電子伝達に関与する元素であり，血液疾患，肝疾患，悪性腫瘍などでは代謝に異常が認められる．鉄代謝に関する情報は，ヘモグロビン，血清鉄，鉄結合能，血中トランスフェリン，血中フェリチンにより得られる．

2）鉄の測定法[5,7]

ヘモグロビン，血清鉄，鉄結合能の測定には比色法，原子吸光法，ICP発光分析法が，トランスフェリン，フェリチンの測定には免疫測定法が用いられる．日常臨床検査における血清鉄測定では，比色法が汎用されている．例えば，試料中の鉄はグロブリン中のトランスフェリンと結合して存在しているが，このトランスフェリン結合鉄をFe^{3+}を酸性下で遊離させ，還元剤(アスコルビン酸)でFe^{2+}に還元し，Fe^{2+}を2-ニトロソ-5-(N-プロピル-N-スルホプロピルアミノ)-フェノールとキレート化合物を形成し発色させ，これを比色定量して血清鉄値を求める手法がある．

3. マグネシウム

1）マグネシウム値の変動と疾病[5,8]

体内のマグネシウムはすべての細胞，骨に分布しているが特に骨(約66%)，脳や筋などに多く存在し，各種酵素の活性化，筋神経系の興奮伝達に重要な元素である．マグネシウム代謝の全貌は未だ不明な点があるが，摂取不足や嘔吐，下痢等により体内からマグネシウムが欠乏すると，腎における再吸収が促進する．マグネシウム欠乏の診断には血中(血清，血球)，尿中マグネシウム濃度を用いる．ただし，尿中濃度の測定には，日内変動を考慮し，起床後2回目の尿を試料とする．一方，高マグネシウム血症は腎機能障害の場合に認められ，血清マグネシウム濃度により判定される．

2）マグネシウムの測定法[5]

日常的なマグネシウム濃度の測定法として，色素法，原子吸光法，酵素法が挙げられる．酵素法は特異性が高く，自動分析器に応用し多検体処理が可能である．酵素法としては，イソクエン酸脱水素酵素(ICDH)を利用したものがあり，ICDHの活性は検体中のマグネシウム濃度に依存することを利用したもので，イソクエン酸，ニコチンアミドアデニンジヌクレオチドリン酸(NADP)の存在下で検体中のマグネシウムによって活性化したICDHを反応させ，このときに生成するNADPHの吸光度の増加量を測定することによって，検体中のマグネシウム濃度を決定している．色素法としては，試料中のマグネシウムが，アルカリ条件下においてキシリルアゾバイオレットと結合して赤色のキレート化合物を形成することを利用し，この赤色の吸光度を測定することによりマグネシウム濃度を測定する方法(キシリジルブルー法)がある．マグネシウムに関しての正確な測定には，やはり原子吸光法が断然優位である．

4. 銅

1）銅値の変動と疾病[5,9]

体内の銅は，骨，筋，肝，脳等に多く分布し，造血や結合組織の代謝に不可欠な元素である．血清中の銅は約95%がセルロプラスミンと結合していることから，セルロプラスミン濃度は血清銅を反映していると言える．Wilson病は，銅輸送蛋白質の遺伝子異常に起因し，血清銅濃度の低下，およびアルブミンやヒスチジンなどのアミノ酸結合銅濃度の増加を認める先天性疾患である．一方，炎症や妊娠により，血清銅濃度は増加する．

2）銅の測定法[5]

原子吸光法，および比色法が挙げられる．比色法は，血清などの試料に還元剤を含む希塩酸などを加え，蛋白質から銅を遊離する．さらに2価の銅から1価に銅は還元され，バソクプロインスルホン酸とキレートし，橙黄色を呈することから，これを比色するバソクプロイン法や3，5-DiBr-PAESAとキレートさせる方法が利用されている．

5. 亜鉛

1）亜鉛値の変動と疾病[5,10]

亜鉛は，種々の酵素のコファクターとして機能し，特定の受容体に対する核内受容体におけるZnフィンガーの構成元素として存在することから，生命維持に不可欠な元素である．したがって，亜鉛の生体内レベルは重要な情報である．亜鉛欠乏の判定は摂取不足，吸収阻害を反映する血清濃度と，体液中に比較的高濃度に亜鉛が存在することから，尿中排泄量を併せて検討する方が適切である．欠乏症状として，生殖機能の低下，成長停止，創傷治癒障害，脱毛，味覚嗅覚の低下，食欲低下などが認められる．

2）亜鉛の測定法[5]

原子吸光法と比色法が存在するが，比色法は精度に問題があるといわれている．比色法として，試料にトリクロロ酢酸を加え，除蛋白後，2-(5-ブロモ-2-ピリジルアゾ)-5-(*N*-プロピル-*N*-スルホプロピルアミノ)フェノールナトリウム(5-Br-PAPS)とキレートさせ，赤紫色のキレートを吸光度測定するものである．一般的には，精度の問題からため，原子吸光法を利用するほうが良い．

おわりに

様々な微量元素と種々の疾病とのかかわりが明らかになっていく中，日常診断，治療の現場における微量元素のモニタリングの必要性が高まってきている．微量元素のほとんどは，生体内での存在量が微量であり，高感度な機器分析では測定に供する前処理や器具の汚れによるコンタミネーションに十分に留意する必要がある．先端分析技術の導入においては，その高感度性を十二分に発揮するためには，データの信頼度を高める操作技術の習得も重要である．

文　献

1）金井泉，金井正光：臨床検査法提要改定第31版，金原出版，1998
2）原口紘炁：ICP発光分析の基礎と応用，講談社サイエンティフィック，1986
3）小椋康光，鈴木和夫：スペシエーション．生命元素事典(桜井弘編)，オーム社，pp 352-358，2006
4）廣村信，五十嵐香織，榎本秀一：ミネラルのイメージング技術．ミネラルの科学と最新応用技術(糸川嘉則監修)，シーエムシー出版，pp 397-419，2008
5）野本昭三，金井正光：無機質(Ca，Mg，P，Fe，Cu，Zn)の測定．臨床検査法提要改定第31版(金井正光編)，金原出版，pp 587-605，1998
6）渡邊光安，相澤好治：鉄．ミネラルの事典(糸川嘉則編)，朝倉書店，pp 220-222，2003
7）廣田俊：鉄．生命元素事典(桜井弘編)，オーム社，pp 78-81，2006
8）西牟田守：マグネシウム．ミネラルの事典(糸川嘉則編)，朝倉書店，pp 205-219，2003
9）児玉浩子：ウィルソン病・メンケス病と銅代謝．生命元素事典(桜井弘編)，オーム社，pp 258-261，2006
10）手塚統夫：栄養．ハーパー生化学　原著25版(上代淑人監訳)，丸善，pp 708-709，2001

Radiochim. Acta 97, 83–89 (2009) / DOI 10.1524/ract.2009.1577

Adsorption of Db and its homologues Nb and Ta, and the pseudo-homologue Pa on anion-exchange resin in HF solution

By K. Tsukada[1,*], H. Haba[2], M. Asai[1], A. Toyoshima[1], K. Akiyama[3], Y. Kasamatsu[1], I. Nishinaka[1], S. Ichikawa[1], K. Yasuda[1], Y. Miyamoto[1], K. Hashimoto[1], Y. Nagame[1], S. Goto[4], H. Kudo[4], W. Sato[5], A. Shinohara[5], Y. Oura[3], K. Sueki[6], H. Kikunaga[5], N. Kinoshita[7], A. Yokoyama[8], M. Schädel[9], W. Brüchle[9] and J. V. Kratz[10]

[1] Advanced Science Research Center, Japan Atomic Energy Agency (JAEA), Tokai, Ibaraki 319-1195, Japan
[2] Nishina Center for Accelerator Based Science, RIKEN, Wako, Saitama 351-0198, Japan
[3] Department of Chemistry, Tokyo Metropolitan University, Hachioji, Tokyo 192-0397, Japan
[4] Department of Chemistry, Niigata University, Niigata, Niigata 950-2181, Japan
[5] Department of Chemistry, Osaka University, Toyonaka, Osaka 560-0043, Japan
[6] Department of Chemistry, University of Tsukuba, Tsukuba, Ibaraki 305-8571, Japan
[7] High Energy Accelerator Research Organization (KEK), Tsukuba, Ibaraki 305-0801, Japan
[8] Department of Chemistry, Kanazawa University, Kanazawa, Ishikawa 920-1192, Japan
[9] Gesellschaft für Schwerionenforschung, 64291 Darmstadt, Germany
[10] Institut für Kernchemie, Universität Mainz, 55099 Mainz, Germany

(Received June 10, 2008; accepted in revised form August 4, 2008)

*Dubnium (*Db*) / Anion-exchange chromatography / Hydrofluoric acid / Fluoride complexation / Atom-at-a-time chemistry*

Summary. Anion-exchange chromatography of element 105, dubnium (Db), produced in the $^{248}Cm(^{19}F, 5n)^{262}Db$ reaction is investigated together with the homologues Nb and Ta, and the pseudo-homologue Pa in 13.9 M hydrofluoric acid (HF) solution. The distribution coefficient (K_d) of Db on an anion-exchange resin is successfully determined by running cycles of 1702 chromatographic column separations. The result clearly indicates that the adsorption of Db on the resin is significantly different from that of the homologues and that the adsorption of anionic fluoro complexes of these elements decreases in the sequence of Ta $\approx$ Nb > Db $\geq$ Pa.

1. Introduction

Studies on chemical properties of the transactinide elements with atomic numbers $Z \geq 104$ are extremely interesting and challenging subjects in the fields of modern nuclear and radiochemistry; chemical characterization of these elements explores the new frontiers of the elements in the 7th period of the Periodic Table. From sophisticated experimental investigations so far performed, one can justify placing the elements rutherfordium (Rf) through hassium (Hs) into groups 4 to 8 of the Periodic Table [1–5]. The most recent study on element 112 also suggests this element shows the behavior typical of the group-12 elements [6]. However, some of these experiments show conflicting results and some others are criticized due to unsatisfactory experimental conditions because of the strict restricted experimental conditions on an atom-at-a-time basis [2]. Therefore, it is of great importance to obtain accurate results with good statistics to characterize chemical properties of those elements.

Several attempts to clarify chemical properties of Db in aqueous solution have been made by extraction and ion-exchange chromatography methods [7–13]. Comparative studies of Db with its lighter homologues Nb and Ta, and the pseudo-homologue Pa were carried out. Typical results on the halide complex formation of Db demonstrate that its reversed-phase extraction behavior into aliphatic amines follows closely that of the homologue Nb; it differs considerably from both Pa and Ta in HCl, while it differs mostly from the behavior of Pa in HF [12]. For the distribution coefficient (K_d) of Db in 4 M HF [12], however, only a lower limit was measured, so that a clear distinction in fluoride complexation among those elements has not been established. In our previous works [14–19], the fluoride complexation of Rf belonging to the group-4 elements was investigated through anion- and cation-exchange chromatography together with the lighter homologues Zr and Hf, and the pseudo-homologue Th in HF and in HF/HNO_3 mixed solutions. Those results revealed that the ion-exchange behavior of Rf is remarkably different from that of the homologues, and that the fluoride complexation of Rf is much weaker than that of Zr and Hf, but it is stronger than the complexation of Th.

The present study aims at experimentally determining the K_d of Db on anion-exchange resin in HF and to compare the adsorption of Db with that of the homologues. To find suitable experimental conditions for Db, we first measured K_d values of Nb, Ta, and Pa on anion-exchange resin in 0.97–26.4 M HF through batch experiments using the long-lived radiotracers ^{92m}Nb, ^{177}Ta, and ^{233}Pa. Then, the on-line anion-exchange behavior of ^{262}Db, ^{170}Ta, ^{178m}Ta, and ^{90}Nb was investigated by column chromatographic methods with the Automated Ion-exchange separation apparatus coupled with the Detection system for Alpha spectroscopy,

*Author for correspondence (E-mail: tsukada.kazuaki@jaea.go.jp).

AIDA [16, 20]. The K_d value of Db was successfully determined in 13.9 M HF where the adsorption strength of the anionic fluoro complex of Db is comparable to those of Nb, Ta, and Pa.

2. Experimental

2.1 Batch experiments

The radiotracers ^{92m}Nb ($T_{1/2} = 10.15$ d) and ^{177}Ta ($T_{1/2} = 56.56$ h) were produced *via* the ^{92}Zr(p, n) and ^{177}Hf(p, n) reactions, respectively, by bombarding ^{nat}Zr (65.1 mg cm^{-2}) and ^{nat}Hf (141 mg cm^{-2}) metallic foils at the JAEA tandem accelerator and the RIKEN K70 AVF Cyclotron (nat: natural isotopic abundance). The target materials were dissolved in concentrated HF and the solution was evaporated to dryness. Then, the residue was dissolved in 1.0 M HF and was fed onto an anion-exchange column (Dowex 1 × 8, 200–400 mesh, 7 mm i.d. × 10 mm). The ^{92m}Nb tracer was eluted with 5.0 M HNO_3 and 0.2 M HF mixed solution, while ^{177}Ta was eluted with 26.4 M HF. Protactinium-233 ($T_{1/2} = 27.0$ d) was prepared as an α-decay product of ^{237}Np; ^{233}Pa was separated from ^{237}Np on an anion-exchange column with 9.0 M HCl and 0.025 M HF mixed solution. These radiotracers were stored in polypropylene vessels in 1.0 M HF solution.

For the batch-wise experiments, the anion-exchange resin used was MCI GEL CA08Y, supplied by Mitsubishi Chemical Corporation, a strongly basic quaternary-amine polymer with a particle size of 22 ± 2 μm. The commercially available CA08Y in the chloride form was converted to the fluoride one by washing the column with concentrated HF. Then, the resin was washed thoroughly by the batch method with H_2O and was dried up to a constant weight at 80 °C in a vacuum oven. A portion of 10–15 mg of the resin and 3 mL of the 0.96–26.4 M HF solution containing 50 μL of the tracer solution were added into a polypropylene tube and were shaken for 60 min at 20 °C. After centrifugation, 1.0 mL of the aqueous phase was precisely pipetted into a polyethylene tube and subjected to γ-ray spectrometry using a Ge detector. As a reference sample, 50 μL of the tracer solution was diluted to 1.0 mL with 0.1 M HF in another polyethylene tube. Control experiments without the CA08Y resin were also carried out to evaluate adsorption of the tracers on the inner wall of the polypropylene tube. The number of ^{92m}Nb, ^{177}Ta, and ^{233}Pa atoms used for each batch experiment was 10^{10}–10^{11}. The concentration of HF was determined by titration with a standardized NaOH solution. The details of the preparation of the radiotracers and of the batch-wise experiments are described in a separate paper [21].

2.2 On-line chromatographic experiments with Nb, Ta, and Zr

To investigate the column chromatographic behavior of Nb and Ta on anion-exchange resin, ^{90}Nb ($T_{1/2} = 14.6$ h) and ^{178m}Ta ($T_{1/2} = 9.31$ min) were simultaneously produced *via* the ^{nat}Zr(p, n) and ^{nat}Hf(p, n) reactions, respectively. Each target of about 100 μg cm^{-2} thickness and 7 mm diameter was electrodeposited on a 5.4 mg cm^{-2} aluminum backing. A stack of target foils, three for each ^{nat}Zr and ^{nat}Hf set in a multiple-target chamber, was irradiated with an 11.3-MeV proton beam with an intensity of 2 μA delivered from the JAEA tandem accelerator. The beam passed through two 4.2 mg cm^{-2} HAVAR vacuum windows and 0.2 mg cm^{-2} of helium cooling gas before entering the target chamber. Reaction products recoiling out of the targets were stopped in helium gas (90 kPa), attached to KCl aerosols generated by sublimation of KCl powder at 640 °C and were continuously transported through a Teflon capillary (2.0 mm i.d. × 28 m long) by a He/KCl gas-jet system to the chemistry laboratory. The same experiment using the nuclide ^{89m}Zr ($T_{1/2} = 4.16$ min) produced in the ^{89}Y(p, n) reaction was also conducted to monitor the chromatographic behavior of the group-4 element Zr under identical conditions. To this end, an ^{89}Y metallic foil (112 mg cm^{-2}) was bombarded by the proton beam from the JAEA tandem accelerator.

On-line anion-exchange chromatography was performed using AIDA which consists of a modified ARCA [22] and an automated on-line α-particle detection system [16, 20]. The reaction products transported by the He/KCl gas-jet system were deposited on the collection site of AIDA. After deposition for 180 s, the reaction products were dissolved in 8.0–26.1 M HF and were loaded onto 1.0 mm i.d. × 3.5 mm chromatographic columns filled with the MCI GEL CA08Y resin at a flow rate of 1.2 mL min^{-1}. The effluent fractions were consecutively collected in 8 polyethylene tubes and were assayed by γ-ray spectrometry with Ge detectors to obtain elution curves for Nb, Ta, and Zr. The number of ^{90}Nb, ^{178m}Ta, and ^{89m}Zr atoms present in the anion-exchange experiments was about 10^6.

2.3 On-line chromatographic experiments with Db and Ta

The isotope ^{262}Db ($T_{1/2} = 34$ s) was produced *via* the ^{248}Cm(^{19}F, 5n) reaction. The ^{248}Cm material (97.5% ^{248}Cm) was purified by cation- and anion-exchange separation methods to remove impurities. The ^{248}Cm target of 600 μg cm^{-2} thickness and 5 mm diameter was prepared by electrodeposition of $Cm(NO_3)_3$ in 2-propanol onto a 2.1 mg cm^{-2} beryllium backing foil. To compare the behavior of Db with that of the homologue Ta, the chemical experiment of Db was conducted together with Ta. Therefore, Gd (39.3%-enriched ^{152}Gd of 36 μg cm^{-2} thickness) was admixed in the ^{248}Cm target to simultaneously produce ^{170}Ta ($T_{1/2} = 6.76$ min). The 119.2-MeV ^{19}F beam with an intensity of approximately 280 particle nA delivered from the JAEA tandem accelerator passed through a HAVAR vacuum window (1.8 mg cm^{-2}), helium cooling gas (0.09 mg cm^{-2}), the beryllium target backing, and finally entered the target material at the energy range of 102.1–103.6 MeV. At this incident energy, the excitation function for the ^{248}Cm(^{19}F, 5n)^{262}Db reaction exhibits a maximum cross section of 1.5 ± 0.4 nb [23]. This results in an expected production rate of about 0.4 atoms per minute under the present conditions. The transport efficiency of the gas-jet system was estimated to be 30–35% [23].

On-line anion-exchange chromatography was performed using AIDA. The reaction products transported by the He/KCl gas-jet system were deposited on the collection site of AIDA for 75 s. Then, the products were dissolved in

110 μL of 13.9 M HF solution and were fed onto the chromatographic column (1.0 mm i.d. × 3.5 mm) at a flow rate of 1.2 mL min^{-1} that corresponds to 6 column volumes per second. The effluent was collected on a tantalum disk as fraction 1 and evaporated to dryness using hot helium gas and a halogen heat lamp. The remaining products in the column were stripped with 120 μL of 6.0 M HNO_3 and 0.015 M HF mixed solution at a flow rate of 1.0 mL min^{-1}. We confirmed that the above mentioned HF solution was sufficient to strip 100% of Nb and over 80% of Ta from the used anion-exchange column. The 6.0 M HNO_3/0.015 M HF effluent was collected on another tantalum disk and was evaporated to dryness as fraction 2. Both tantalum disks were automatically transferred to an α-spectrometry station equipped with eight 600 mm^2 passivated ion-implanted planar silicon (PIPS) detectors. The chromatographic separation was accomplished within 29 s and the α-particle measurement was started at 53 s and 68 s for each fraction after the collection of the products. The duration of the measurement was 238 s and 223 s for fraction 1 and 2, respectively. Spontaneous fission decay of ^{262}Db was not measured in the present study. Every step of the separation and measurement was controlled by a computer and we repeated these separation processes 1702 times with AIDA. Counting efficiencies of each detector ranged from 30–40% depending on geometrical differences of the dried sources, and the α-particle energy resolution was 100–200 keV FWHM. All events were registered event by event together with time information. After the α-particle measurement, the 221 keV γ-radiation of ^{170}Ta in every fifth pair of the samples was monitored with Ge detectors to determine the elution behavior of Ta and its chemical yield. The chemical yield of ^{170}Ta including deposition and dissolution efficiencies of the aerosols was approximately 55%.

3. Results and discussion

3.1 Batch experiments

The distribution coefficient (K_d) in units of mL g^{-1} of the atoms in question between the resin and the solution is expressed using the following equation:

$$K_d = \frac{A_r V_s}{A_s W_r}, \quad (1)$$

where A_r and A_s are the radioactivities in the resin and the solution, respectively, V_s is the volume of the acid solution (mL) and W_r the mass of the dry resin (g). In Fig. 1, the variation of the K_d values of ^{92m}Nb, ^{177}Ta, and ^{233}Pa on CA08Y is shown as a function of the initial HF concentration, $[HF]_{ini}$: log K_d vs. log $[HF]_{ini}$. The log K_d values of Nb and Ta linearly decrease with an increase of log $[HF]_{ini}$ up to around 11 M with the slopes of -2.3 ± 0.1 and -2.5 ± 0.1, respectively, while that of Pa decreases with the slope of -2.8 ± 0.1 in the studied $[HF]_{ini}$: 0.96 M $\leq [HF]_{ini} \leq$ 26.4 M. It is well known that HF is equilibrated among the following species HF, H^+, F^-, and HF_2^- in the solution and that at $[HF]_{ini} > 1$ M, the concentration of the anionic HF_2^- species is the dominant one [24]. Thus, the decrease of the log K_d values of these elements with log $[HF]_{ini}$ is interpreted as the displacement of metal fluoro complexes from the binding sites of the resin by the counter anion HF_2^-.

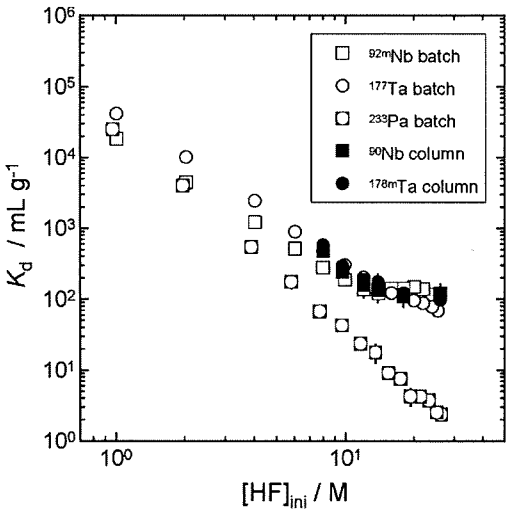

Fig. 1. Variation of the distribution coefficient, K_d, of ^{92m}Nb, ^{177}Ta, and ^{233}Pa on the anion-exchange resin CA08Y as a function of the initial HF concentration, $[HF]_{ini}$. The K_d values of ^{90}Nb and ^{178m}Ta obtained from the on-line column experiment are also shown.

Similar anion-exchange experiments with Nb, Ta, and Pa [24–31], and spectroscopic studies of Nb and Ta [32, 33] were carried out to elucidate chemical species of these elements in HF. The results show that the anionic complex of $[NbOF_5]^{2-}$ is stable at $[HF]_{ini} \leq 10$ M, while $[NbF_6]^-$ and $[NbF_7]^{2-}$ are formed at around $[HF]_{ini} > 10$ M. The sudden change of the slope for Nb in Fig. 1 suggests the transformation of the chemical species from the oxo-fluoro complex to the fluoride ones as reported by Caletka and Krivan [28]. A small change of the slope for Ta is also seen above $[HF]_{ini} \approx 15$ M. It has been reported that Ta forms in HF fluoro complexes of the form: $[TaF_6]^-$, $[TaF_7]^{2-}$, $[TaF_8]^{3-}$ and $[TaF_9]^{4-}$, and that Pa is present in the form of the anionic species of $[PaF_7]^{2-}$ and $[PaF_8]^{3-}$ in $[HF]_{ini} > 10^{-3}$ M [24–33]. Although we could not definitely identify the anionic fluoro complexes of Nb, Ta, and Pa through the present experiment, the results in Fig. 1 are consistent with those in the literature as summarized by Korkisch [34].

3.2 On-line chromatographic behavior of Nb, Ta, and Zr

In Fig. 2, typical elution curves of ^{90}Nb and ^{178m}Ta simultaneously produced in the proton-induced reactions on ^{nat}Zr and ^{nat}Hf, respectively, in 9.7, 13.9 and 26.1 M HF are depicted. According to the Glückauf formula of chromatography [35], the eluted radioactivity $A(v)$ with the effluent volume v is represented by the following equation:

$$A(v) = A_{max} \exp\left\{-\frac{N}{2}\frac{(v_p - v)^2}{v_p v}\right\}, \quad (2)$$

where parameters A_{max}, N, and v_p are the maximum peak height, the number of theoretical plates, and the peak volume, respectively. It is noted here that the v and v_p values are corrected for the dead volume (24 μL) of the present column. The results of the fit by Eq. (2) are drawn by dashed,

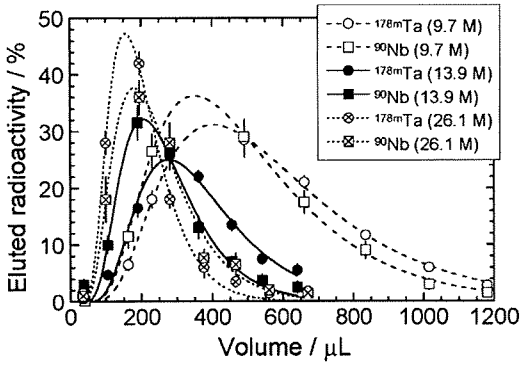

Fig. 2. Elution curves of ^{90}Nb and ^{178m}Ta in 9.7, 13.9, and 26.1 M HF at a flow rate of 1.2 mL min^{-1}. The curves indicate the results of the fits by the Glückauf equation [35].

solid, and dotted curves in Fig. 2 for each condition, showing good agreement between the experiments and the equation. The number of theoretical plates N was evaluated to be 4.5 ± 0.5. In the column chromatographic system, the K_d value is described as

$$K_d = \frac{v_p}{m_r}, \quad (3)$$

where m_r is the mass of the dry resin. The average m_r value was measured to be 1.3 ± 0.1 mg. The K_d values evaluated from the column method are also plotted in Fig. 1 and agree well with those from the static batch ones. This indicates that the anion-exchange processes taking place in the present column experiment reach equilibrium.

3.3 On-line chromatographic behavior of Db and Ta at 13.9 M HF

Based on the above batch and on-line column experiments, the chromatographic experiment of Db was conducted at $[HF]_{ini} = 13.9$ M where the K_d values of Nb/Ta are remarkably different from that of Pa. It should be interesting to observe how Db behaves on the anion-exchange resin: Nb/Ta-like or Pa-like. Further, the range of the measurable K_d values with the present AIDA system is limited by the size of the micro column (1.0 mm i.d. × 3.5 mm) to be 20 to 200. Therefore, we performed the on-line column experiment with Db at 13.9 M HF.

1702 anion-exchange experiments were conducted with AIDA. The sum of α-particle spectra of samples prepared from the two effluents, fractions 1 and 2, are shown in Fig. 3a and b, respectively. The total beam dose of ^{19}F was 2.2×10^{17} particles. The isotope ^{244}Cm, a recoil product of the target (the isotopic composition of the ^{248}Cm target is as follows: ^{244}Cm (1.12 at.%) and ^{246}Cm (1.31 at.%)), and the Fr isotopes, transfer reaction products, are mostly eluted with 13.9 M HF. As listed in Table 1, a total of 10 α events from 34-s ^{262}Db ($E_\alpha = 8.45$, 8.53 and 8.67 MeV) [36] and its daughter 3.9-s ^{258}Lr ($E_\alpha = 8.57$, 8.60, 8.62 and 8.65 MeV) [36] were registered in the energy range of 8.25–8.68 MeV, including 2 time-correlated α pairs of ^{262}Db and ^{258}Lr. The life-times of the α-decay events arising from ^{262}Db and ^{258}Lr are also listed in Table 1. The evaluated average life-time of 52.9 s resulted in a half-life of about 36.7 s that is compatible with the sum of the individual half-lives of ^{262}Db and ^{258}Lr (two of these events are ascribed

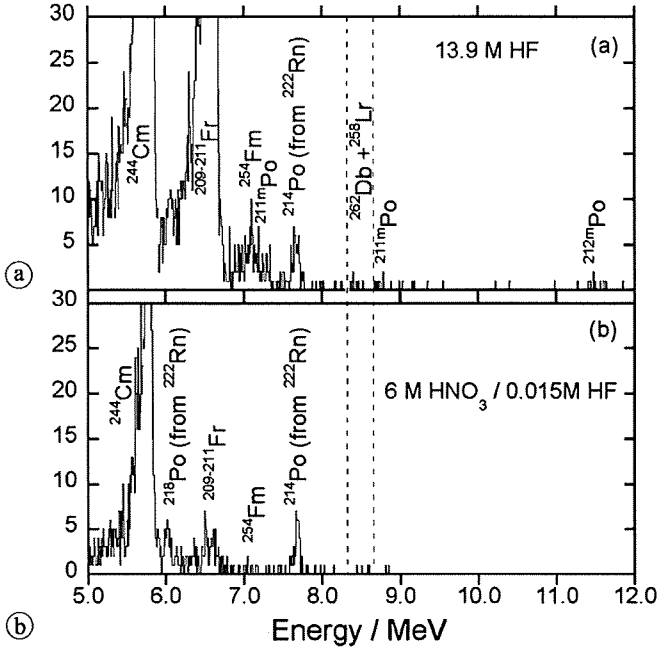

Fig. 3. Sum of α-particle spectra prepared from the two effluents: (**a**) 13.9 M HF and (**b**) 6 M HNO_3/0.015 M HF. The vertical dashed lines show the gated energy range for the analysis: 8.25–8.68 MeV.

Table 1. Observed α events in the energy range of 8.25 to 8.68 MeV.

Event No.	Fraction No.	Energy (MeV)	Life-time (s)	Remarks
1	2	8.584	71.5	
2	2	8.446	10.5	Mother
3	2	8.613	16.9	Daughter ($\Delta T = 6.4$ s)
4	1	8.449	9.4	
5	1	8.414	92.8	Mother
6	1	8.484	98.7	Daughter ($\Delta T = 5.9$ s)
7	1	8.363	142.1	
8	1	8.266	59.4	
9	1	8.382	10.1	
10	2	8.592	17.6	

to background counts as mentioned below). From the time difference ΔT between the correlated α-decay events, we obtained an average life-time of 6.2 s for the daughter nuclide ^{258}Lr.

The average background count rate from cosmic rays and electronic noise, *etc.*, was determined in a long counting interval as 3.2×10^{-6} counts s^{-1} for each detector in the α-particle energy range of interest. The total background counts resulted in 1.3 and 1.2 for fraction-1 and fraction-2, respectively. The probability of the random correlation rate was evaluated to be less than 7.4×10^{-4} during the measurement (1702×238 s and 1702×223 s for fractions 1 and 2, respectively), while the singles events subtracting the background resulted in 7.5. The event ratio between the total α counts and α–α correlations was estimated to be 10 : 1.7, taking into consideration the counting efficiency of the detector (35%), the recoil effect of ^{258}Lr, and the decay of ^{262}Db and ^{258}Lr. The observed ratio of 7.5 : 2 is reasonably consistent with the estimated one within the counting statis-

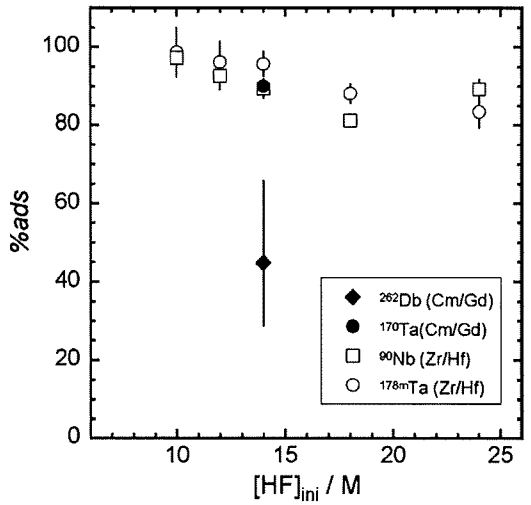

Fig. 4. Variation of the adsorption probability, % ads, of Nb, Ta, and Db on the anion-exchange resin CA08Y obtained from the on-line column experiments as a function of the initial HF concentration, $[HF]_{ini}$. The data of ^{262}Db and ^{170}Ta obtained from the Cm/Gd target are shown by closed symbols, while those of ^{90}Nb and ^{178m}Ta from the Zr/Hf targets are shown by open ones.

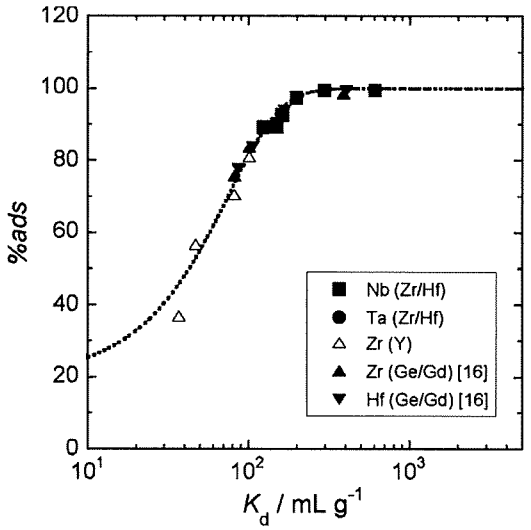

Fig. 5. Variation of the adsorption probability, % ads, of Nb and Ta produced from the Zr/Hf targets on the anion-exchange resin CA08Y as a function of the distribution coefficient, K_d. The data of Zr produced from ^{89}Y(p, n) are depicted by open triangles. The % ads values of Zr and Hf produced from the Ge/Gd targets taken from [16] are shown by closed triangles and inverse triangles, respectively.

tics. The evaluated production cross section of ^{262}Db based on the total α-events of 7.5 was about 1 nb by assuming the α-decay branch of $I_\alpha = 64\%$ in ^{262}Db [36] that is consistent with the previous value in [23].

From the radioactivities A_1 and A_2 measured in fractions 1 and 2, respectively, the adsorption probability (% ads) on CA08Y was evaluated using the relation: $\%\,\text{ads} = 100A_2/(A_1 + A_2)$. The corrections for the radioactive decay and the background were considered for A_1 and A_2. Because of the short half-life of ^{258}Lr, the contribution of ^{258}Lr formed from ^{262}Db during the collection before the chemical separation was not taken into account. The % ads values of ^{262}Db and ^{170}Ta were $45^{+21}_{-16}\%$ and $90 \pm 2\%$, respectively, as shown in Fig. 4. The error limits of the % ads value of ^{262}Db was evaluated from the counting statistics of the observed α events based on the 68% confidence intervals for Poisson distributed variables [37]. The % ads values of ^{90}Nb and ^{178m}Ta produced from the Zr/Hf target in the separate run are also depicted in Fig. 4 as a function of $[HF]_{ini}$. It should be noted here that the data of Ta from both runs are in good agreement. It is clearly seen that the % ads value of Db is much smaller than those of Nb and Ta.

The K_d value of Db was evaluated by assuming that the kinetics in the complexation and ion-exchange processes of Db is as fast as those for the homologues as described in [16, 17]. In Fig. 5, the correlation between the % ads and K_d values of Nb and Ta are plotted together with the data of Zr produced in ^{89}Y(p, n) and those of Zr and Hf taken from [16]. The % ads values of those elements are found to be smoothly correlated with K_d,

$$\%\,\text{ads} = 100 \exp\left[-a \exp\{-b(K_d - c)\}\right]. \quad (4)$$

The % ads value of Db from the column method can be transformed into the K_d value using Eq. (4). The obtained K_d is shown in Fig. 6 together with those of Nb, Ta, and Pa obtained from the batch experiment. The K_d values of the group-4 elements, Zr, Hf, and Rf taken from Ref. [16], are

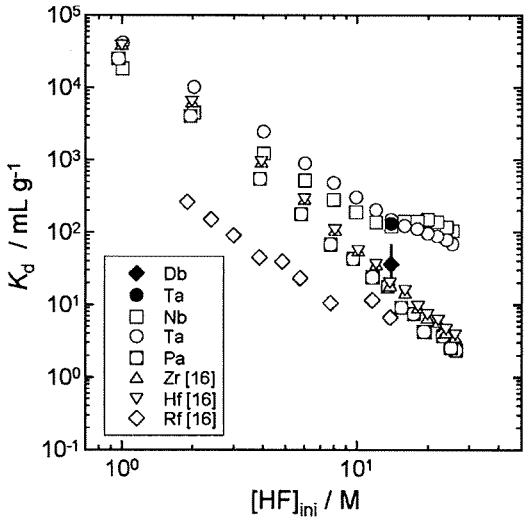

Fig. 6. Variation of the distribution coefficient, K_d, of Db, Nb, Ta, and Pa on the anion-exchange resin CA08Y as a function of $[HF]_{ini}$. The values of Db and Ta obtained from the on-line column experiment are indicated by closed symbols, while those of Nb, Ta and Pa obtained from the batch experiment are shown by open symbols. The K_d values of Rf, Zr and Hf taken from Ref. [16] are also plotted.

also plotted. The errors associated with ^{262}Db are propagated from the error limits of the % ads value. As seen from Fig. 6, the K_d value of Db is significantly smaller than those of Nb and Ta at $[HF]_{ini} = 13.9$ M, while it is larger than that of Pa. The result demonstrates that the adsorption of these elements is in the sequence of Ta $\approx$ Nb > Db $\geq$ Pa. The present result is not contradictory to that in the amine extraction study of Db at 4 M HF [12]. The lower limit value of K_d in [12] would be beyond the limit of measurable K_d values with the micro columns.

As shown in Fig. 6 and described in [14–19], it has been found that the fluoride complexation of Rf is significantly weaker than that of Zr and Hf, but it is stronger than